

University of Nevada, Reno

## **Effect of the Mn Additive on Cu-Zn-Al Shape Memory Alloy**

A thesis submitted in partial fulfillment of the  
requirements for the degree of Master of Science in  
Material Science and Engineering

by

Haohan Li

Dr. Qizhen Li/ Thesis Advisor

Dec, 2012

© by Haohan Li 2012  
All Rights Reserved



THE GRADUATE SCHOOL

We recommend that the thesis  
prepared under our supervision by

**HAOHAN LI**

entitled

**Effect of the Mn Additive on Cu-Zn-Al Shape Memory Alloy**

be accepted in partial fulfillment of the  
requirements for the degree of

**MASTER OF SCIENCE**

Qizhen Li, Ph. D. , Advisor

Ravi Subramanian, Ph. D. , Committee Member

Maurice C. Fuerstenau, Ph. D. , Graduate School Representative

Marsha H. Read, Ph. D., Dean, Graduate School

May, 2012

## Abstract

This thesis has reviewed the development and the current status in the research field of copper-based shape memory alloys including the Cu-Al-Ni, Cu-Zn-Al, Cu-Al-Mn, Cu-Al-Be, and other copper-based shape memory alloy. From the standpoint of mechanisms (phase transformation, thermodynamics) and properties (shape memory effect, mechanical properties), this thesis summarizes the previous research and contributions to improve the properties of copper-based shape memory alloys.

A polycrystalline Cu-Zn-Al shape memory alloy was developed and studied. The grain refinement, eutectic structure, and the precipitates were investigated. The microstructure of the alloy has been observed and analyzed; grains are significantly refined by the addition of manganese. The lamellar structure of the alloy has also been discussed. The shape memory effects were evaluated with bending tests, and the results indicate that for the sample without any addition of Mn, the shape recovery is 7°, and for the alloy with 1 % Mn, 5°. The shape memory effect of the newly developed alloy was not significantly decreased although the grains were dramatically refined. The phase transformation procedure and the solidification process were explored; the heat treatment was discussed, and the oxidation and diffusion of the alloy were scrutinized.

## Acknowledgements

I would like to thank Prof. Qizhen Li for her guidance on this research as well as my committee members: Prof. Maurice C. Fuerstenau, Prof. Ravi Subramanian. I also want to thank James Murphy for allowing the usage of the induction furnace and Dr. Mojtaba Ahmadian-Tehrani for allowing us to use the scanning electron microscopy.

I would like to thank my group-mates: Henry Vin Cay, Xing Jiao, Huiru Xu and especially Guiying Rao, for their assistance, as well as my parents for their continuing support.

## Table of Contents

Abstract.....	i
Acknowledgements.....	ii
List of Tables .....	v
List of Figures .....	vi
1. Background .....	1
1.1 Shape memory alloys (SMAs) and Cu-based SMAs .....	1
1.2 Application of the Cu-based SMAs:.....	1
1.3 Property of the Cu-based SMA: .....	2
1.3.1 Superelasticity (SE) or pseudoelasticity (PE).....	2
1.3.2 Electronic concentration (e/a) .....	3
1.3.3 Shape memory effect (SME) or One-way shape memory effect (OWSME) .....	3
1.3.4 Two-way shape memory effect (TWSME) .....	4
1.3.5 Mechanical properties: .....	6
1.3.6 Thermal stability properties.....	6
1.4 Principle: Martensitic transformation within the Cu alloy .....	8
1.5 Sample fabrication .....	11
2. Literature review.....	13
2.1 Cu-Al-Ni shape memory alloys.....	13
2.1.1 Phase and phase transformation investigation: .....	18
2.1.2 Grain refinement:.....	20
2.1.3 Mechanical alloying .....	23
2.1.4 Others .....	24
2.2 Cu-Zn-Al system .....	24
2.3 Cu-Al-Mn system.....	35
2.4 Cu-Al-Be system .....	38
2.4.1 Phase and phase transformation investigation: .....	38
2.4.2 Property improvement: .....	39
2.4.3 Other methods:.....	39
2.5 Other systems .....	40
2.6 Conclusions .....	40

3. Experimental .....	41
3.1 Experiment objectives .....	41
3.1.1 Composition effect.....	41
3.1.2 Structure hardening:.....	42
3.1.3 Electronic density (e/a).....	43
3.2 Device setup.....	44
3.3 Parameter evaluation and assessed: .....	45
3.4 Rolling process evaluation: .....	51
3.5 Heat treatment .....	54
3.6 Experiment details .....	60
4. Results and discussion .....	62
4.1 Comparison of microstructures of different composition.....	62
4.2 Shape memory effect.....	66
5. Conclusions .....	69
Reference:.....	71
Appendix .....	82

## List of Tables

Table 1 Properties of some common Cu-based SMAs.....	6
Table 2 Rolling parameters.....	49
Table 3 Composition of the experiment samples.....	57

## List of Figures

Figure 1. Schematic diagram of one-way shape memory effect.....	4
Figure 2. Schematic diagram of two-way shape memory effect.....	5
Figure 3. Schematic diagram of the bending test on the shape memory effect.....	5
Figure 4. Schematic diagram of the $L_{21}$ (Heulers structure) .....	8
Figure 5. Schematic diagram of $DO_3$ superlattice structure.....	9
Figure 6. Schematic diagram of the 2H structure .....	9
Figure 7. Evolution of the 18R in the monoclinic (M18R) from the $DO_3$ superlattice.....	10
Figure 8. Phase diagram for the Cu-Al-Ni with different composition of Al.....	14
Figure 9. Ternary phase diagram of the Cu-Al-Ni at the liquid projection.....	14
Figure 10. Ternary phase diagram of the Cu-Al-Ni at 900 °C.....	15
Figure 11. Ternary phase diagram of the Cu-Al-Ni at 700 °C.....	15
Figure 12. Ternary phase diagram of the Cu-Al-Ni at 500 °C.....	16
Figure 13. Ternary phase diagram of the Cu-Zn-Al at the liquid projection.....	23
Figure 14. Ternary phase diagram of the Cu-Zn-Al at 700 °C.....	23
Figure 15. Ternary phase diagram of the Cu-Zn-Al at 650 °C.....	24
Figure 16. Ternary phase diagram of the Cu-Zn-Al at 600 °C.....	24
Figure 17. Ternary phase diagram of the Cu-Zn-Al at 550 °C.....	25
Figure 18. Ternary phase diagram of the Cu-Zn-Al at 500 °C.....	25
Figure 19. Ternary phase diagram of the Cu-Zn-Al at 400 °C.....	26
Figure 20. Ternary phase diagram of the Cu-Zn-Al at 350 °C.....	26

Figure 21. Ternary phase diagram of the Cu-Zn-Al at 300 °C.....	27
Figure 22. Ternary phase diagram of the Cu-Zn-Al at 240 °C.....	27
Figure 23. Ternary phase diagram of the Cu-Zn-Al at 200 °C.....	28
Figure 24. Phase diagram of Cu-Zn-Al at 700 °C.....	41
Figure 25. Picture of the conventional inert gas protection setup for the induction furnace cast.....	42
Figure 26. Water quenched Cu-Zn-Al alloy sample.....	44
Figure 27. Microstructure of the as-casted eutectic Cu-Zn-Al, x40.....	44
Figure 28. Air cooled as-casted samples of Cu-Zn-Al.....	45
Figure 29. Microstructure of the air cooled Cu-Zn-Al alloy, x80.....	46
Figure 30. Microstructure of the furnace cooling Cu-Zn-Al, x40.....	47
Figure 31. As-rolled Cu-Zn-Al alloy with a rolling reduction percentage of five percent.....	50
Figure 32. As-rolled Cu-Zn-Al alloy with a rolling reduction percentage of three percent.....	51
Figure 33. Schematic diagram of the Matano solution.....	52
Figure 34. Cu-Zn-Al sample after one hour heat treatment and water quenching.....	55
Figure 35. Cu-Zn-Al sample after two hours heat treatment and water quenching.....	55
Figure 36. Cu-Zn-Al sample after four hours heat treatment and water quenching.....	56
Figure 37. Comparison of the one hour heat treatment sample and four hour heat treatment sample.....	56
Figure 38. Stanat double rolling mill.....	58

Figure 39. Schematic diagram of modified shape memory effect bending test.....	59
Figure 40. EDX analysis of the sample 1 (Cu-Zn-Al).....	60
Figure 41. EDX analysis of the sample 2 (Cu-Zn-Al-Mn).....	61
Figure 42. Microstructure of the CZA sample 1 with Cu-Zn-Al, x80.....	62
Figure 43. Microstructure of the sample 2 with Cu-Zn-Al-Mn, x80.....	63
Figure 41. Shape memory effect test of the sample 1 Cu-Zn-Al (deforming stage).....	63
Figure 45. Shape memory effect test of the sample 1 Cu-Zn-Al (Recovering stage).....	64
Figure 46. Shape memory effect test of the sample 2 Cu-Zn-Al-Mn (deforming stage).....	64
Figure 47. Shape memory effect test of the sample 2 Cu-Zn-Al-Mn (recovery stage).....	63

## Chapter 1

### Background

#### 1.1 Shape memory alloys (SMAs)

Shape memory alloys (SMA) refer to those alloys with shape recovery properties. The shape memory effect (SME) enables the alloy to retain the original shape, under specific treatment, such as varying temperatures or stress conditions. When released to the original stress-free condition under thermal, electrical or environmental change, the material tends to recover to their original shape [1]. A further definition is that the SMAs refer to alloys that can transform to thermoelastic martensites. These alloys undergo martensite transformation that allows the alloys to deform by a twinning mechanism, and the deformations are reverted when the twinned structures revert upon heating to the parent phase. This self-accommodation property is defined as the shape memory effect (SME).

#### 1.2 Applications of the Cu-based SMAs

The SMAs were unveiled in 1963 by Buehler et al. when they were developing a new material for heat shielding at the Naval Ordnance Laboratory [1]. Because of their properties, SMAs are highly attractive for various industries, such as the automobile, aerospace, pipeline, and biomedical fields. The existing SMAs are Ni-Ti-, copper-, and ferrous-based SMAs. The universally applied SMAs are Ni-Ti-based due to their good SME and competitive mechanical properties as both structural and functional materials.

However, the cost of these SMAs is higher than that of Cu-based SMAs and Fe-based SMAs. A substituent with a lower cost and similar properties has been sought for decades. Copper-based SMAs, owing to their excellent properties and low cost, have been highly attractive to various industries such as aerospace and aeronautics, automotive, and defense industries. In the recent years, the Cu-based SMAs have been more widely utilized due to its suitability for sensing, impact absorption, and vibration damping applications [2]. In addition, a small sample volume could make the Cu-based SMAs suitable for their use as micro- and even nano-scale actuators because of their capabilities to generate large force and displacement [3].

### 1.3 Properties of the Cu-based SMA

Research has been focused on the properties listed below:

#### 1.3.1 Superelasticity (SE) or pseudoelasticity (PE)

SE or PE is an elastic response to an applied stress, which could result in a reversible deformation under high strain (up to 10 %). When the load is removed, the material tends to recover the original shape without any other environmental change (temperature, magnetic field). Such property is associated with the stress-induced transformation above the Austenite finishing line ( $A_f$ ) [1]. It has been universally recognized that the SE strongly correlates to the grain sizes and is relative to the size of the specimens, the SE increases with the refining of grain size, and the smaller size of the specimens is, the larger SE can be obtained.

This property is generally measured by tensile tests. For SMAs, such a test is usually conducted at a temperature around 30 °C above  $A_f$ . Different strain rates are used, depending on the size and shape of the testing samples.

### 1.3.2 Electronic concentration (e/a)

Electronic concentration refers to the total amount of free electrons in one unit atomic weight. In the binary Cu-Al system, the Cu and Al atoms respectively contribute 1 and 3 electrons to the electronic concentration. Whereas in most cases, a disordered BCC structure can only be obtained at an e/a of 1.4 to 1.55 at high temperature. At a lower temperature, this range is narrowed, and at the eutectic point, the e/a becomes exactly 1.48. Below the eutectic point, the Cu-Al alloy becomes a complex cubic phase with stoichiometry  $\text{Cu}_9\text{Al}_4$  and a disordered FCC phase. Therefore, when cooling down from a high temperature at a fast rate, it is possible to suppress the entire precipitation of the stable phase. In this case, the distorted BCC phase experiences atomic ordering. Detailed ordering will be discussed in the chapter 1.4.

### 1.3.3 Shape memory effect property (SME) or one-way shape memory effect property (OWSME)

OWSME is the property that is generated during austenite transition in the absence of the permanent plastic deformation. In general, after deformed at room temperature, the original shape of SMA can be retained by heating the material up to the austenite temperature, and subsequently, cooling to martensite. This results in the formation of

the self-accommodated twinned martensitic variants and the recovery of the material to the original shape. The shape recovery mechanism is illustrated in Figure 1:

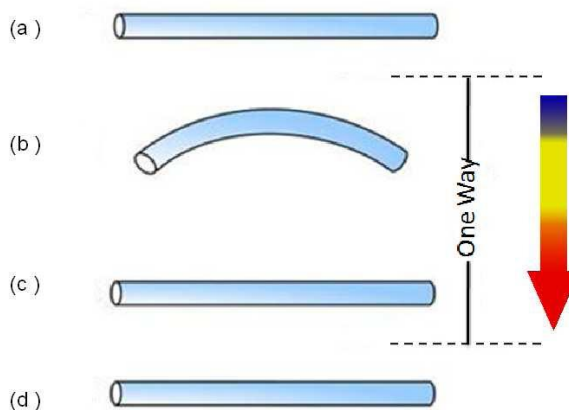


Figure 1. Schematic diagram of one-way shape memory effect [4].

In Figure 1 (a), the material is at room temperature; in Figure 1 (b), the material is deformed at room temperature; in Figure 1 (c), the material is heated up to  $A_f$  without load, and the material recovers to the shape in Figure 1 (a); in Figure 1 (d), the material keeps its recovered shape when been cooled down to room temperature again.

#### 1.3.4 Two-way shape memory effect property (TWSME)

TWSME is the reversible and spontaneous shape change of materials with thermal cycling: the TWSME permits the SMA to have a spontaneous shape change on both heating and cooling stages. Only by changing the temperature can the material undergo change shape with the martensite transformation and austenite transformation [2]. The shape recovery procedures are shown in Figure 2. Generally, such a property can be obtained from the thermomechanical cycling (a process known as “training” in industry

field). This thermomechanical cycling is a series process of deforming and heating alternate with each other.

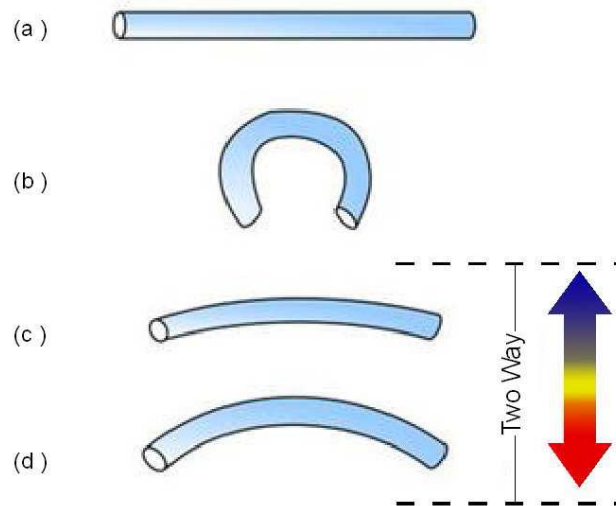


Figure 2. Schematic diagram of two-way shape memory effect [4].

Figure 2 describes the mechanism of TWSME, in Figure 2 (a), the sample was prepared into rod shape, in Figure 2 (b), the sample is deformed at room temperature, in Figure 2 (c) and (d), the sample recovers to its original shape when been heated up (d) and tend to recover to the deformed shape when been cooled down (c).

Both OWSME and TWSME are evaluated by bending test. The test procedures are indicated in Figure 3. The SME can be evaluated by using shape recovery ratio ( $F_{SME}$ ), the Equation (1) shows how the  $F_{SME}$  is defined:

$$F_{SME} = \frac{\theta_M}{(180 - \theta_e)} \times 100 \% [4] \quad Eq. (1)$$

where  $\theta_M$  and  $\theta_e$  can be obtained from Figure 3:

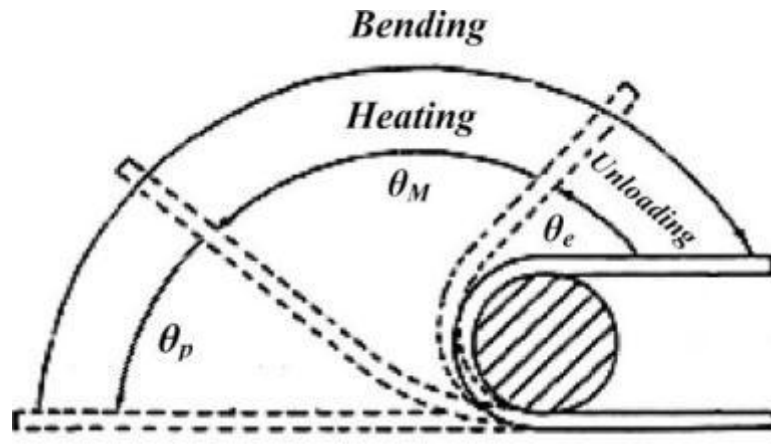


Figure 3. Bending test scheme [4].

From Equation (1), it can be obtained that the  $F_{SME}$  ranges from 0 to 100 %.

In this bending test, samples should be prepared into ribbon shape, no specified standard on dimension have been developed. The author of this thesis chose 2 cm x 0.5 cm in dimension due to producing convenience.

### 1.3.5 Mechanical properties

The mechanical properties refer to the physical deformations (including elongation, compression, twisting, or breaking) that response to the applied stress. The mechanical properties are functions of applied load, time, and temperature.

To test these properties, the most general method is tensile test, bending test and hardness test.

### 1.3.6 Thermal stability properties

Thermal stability is another property that has drawn a lot of interest in the SMAs' investigation. This property describes the stability of a phase at high temperatures and

this property is evaluated by the Differential Scanning Calorimeter (DSC). DSC is used to study thermal stability, and heat associated with the transformation of phase and chemical reactions [5]. Phase identification is usually performed with the X-Ray Diffraction (XRD), Transmission Electron Microscope (TEM) and Scanning Electron Microscope (SEM).

Table 1 [6] shows the properties of some common Cu-based SMAs.

**Table 1. Properties of some common Cu-based SMAs [6].**

Property	Property value	
	Cu-Zn-Al	Cu-Al-Ni
<b>Thermal properties</b>		
Melting point, °C	950-1020	1000-1050
Density, g/cm <sup>3</sup>	7.64	7.12
Resistivity, μΩ·cm	8.5-9.7	11-13
Thermal conductivity, W/m·°C	120	30-43
Heat capacity, J/kg·°C	400	373-574
<b>Mechanical properties</b>		
<i>Young's modulus, GPa</i>		
β phase	72	85
Martensite	70	80
<i>Yield strength, MPa</i>		
β phase	350	400
Martensite	80	130
Ultimate tensile strength, MPa	600	500-800
<b>Shape memory properties</b>		
Transformation temperature, °C	<120	<200
Recoverable strain %	4	4
Hysteresis, Δ°C	15-25	15-20

#### 1.4 Mechanism: Martensitic transformation within the Cu alloy

Martensitic transformation refers to the phase change that occurs without long-range diffusion of atoms.

In terms of the copper-based SMA, a martensite transformation usually refers to a transformation from the distorted BCC structure to the martensite phase. So far, three types of martensites have been identified. They have structures of 6R, 18R and 2H, respectively.

The transformation from the BCC to the above structures is still controversial. It can be confirmed by theory [7] that from the disordered BCC, at a critical ordering temperature, the long range ordering in the first nearest neighbors transform to  $B_2$  (CsCl type) occurs, and this transformation could happen very fast [8]. For some certain chemical composition (the composition factor is be described in Chapter 1.3.2), the long range ordering may take place in the second nearest neighbors. These long-range orderings reconfigure to an  $L_{21}$  structure (Heusler structure, Figure 4). Under different conditions, the three types of martensite can be acquired. For the phase inherited from the  $B_2$  order, the material will first form a  $DO_3$  superlattice (Figure 5), where the martensite is evolved subsequently. The stacking sequences in this case are ABC and ABCBCACAB which are called 3R and 9R, respectively. The formation of the 3R and 9R structures is dependent upon different conditions, including chemical composition (electronic concentration). However, with the presence of  $L_{21}$  order, the stacking is doubled and becomes 6R and 18R structures, respectively. For another situation (if the electronic concentration is

higher than 1.5 in copper-based alloy) inherited from  $B_2$  and  $L_{21}$  orders, an ABAB stacking sequence may be obtained, and a martensite with a structure of 2H can be acquired (the 2H structure is illustrated in the Figure 6). The black balls in Fig 5 and 6 represent Zn in Cu-Zn-Al alloys or Al in Cu-Al-Ni alloys, and the white balls represent Cu in Cu-based SMAs. These three martensites can be considered as a basic Face-centered Tetragonal (FCT) lattice into which stacking faults can be introduced on every third plane for 9R and 18R structures and on every second plane for 2H. In a related literature [9], the parent phase includes all three different structures: disordered BCC, ordered  $B_2$ , and ordered  $L_{21}$  structures. The  $B_2$  transforms into 6M structure while the  $L_{21}$  yields an 18R structure.

Assuming no average distortion at the parent and product interface, the evolution of the 18R structure from the  $DO_3$  structure can be illustrated in Figure 7 [10].

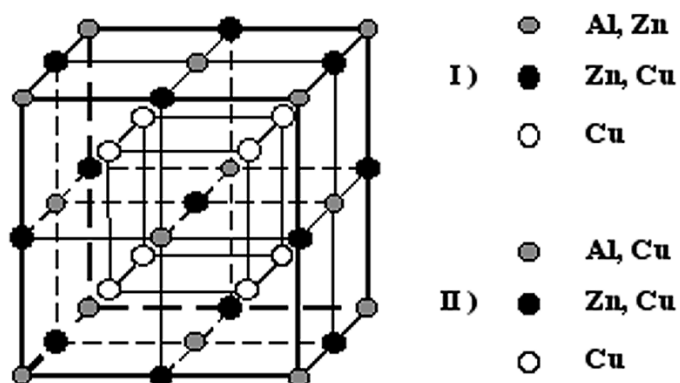


Figure 4. Schematic diagram of  $L_{21}$  (Heulers structure) [7].

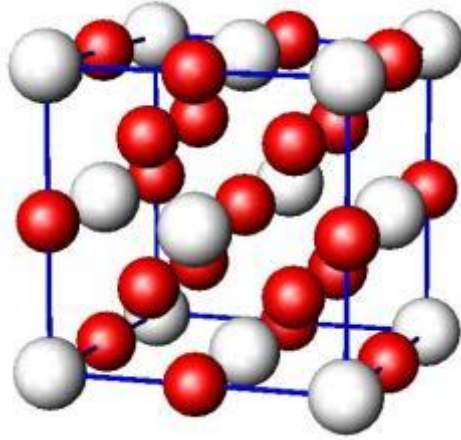


Figure 5. Schematic diagram of DO<sub>3</sub> superlattice structure [8].

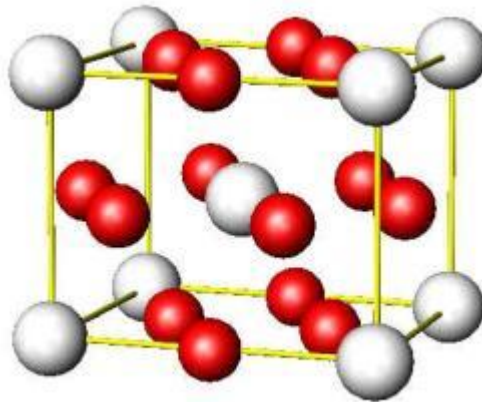


Figure 6. Schematic diagram of 2H structure [8].

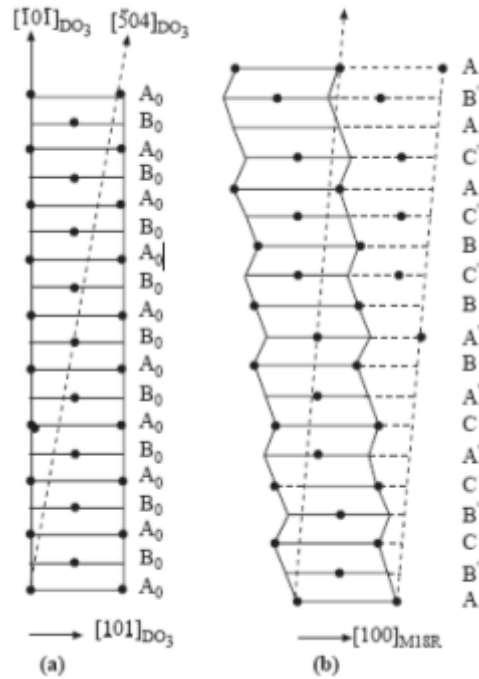


Figure 7. Evolution of the 18R in the monoclinic (M18R) from the DO<sub>3</sub> superlattice [10].

Figure 7 shows the shifting of the original DO<sub>3</sub> structure to the M18R structure by distortion. During the process, the  $[\bar{5}04]$  in the DO<sub>3</sub> structure becomes the  $[001]$  in the M18R structure.

### 1.5 Sample fabrication

There are typically two methods for developing the Cu-based SMAs. They are conventional casting and mechanical alloying.

The conventional casting method involves the addition of all the element precursors into a crucible at a high temperature (above the melting point), so that the materials would diffuse into each other and form the new alloy. Both polycrystalline and single crystalline can be produced with casting method.

The mechanical alloying refers to applying powder metallurgy to fabricate the alloy. Three processes are performed: powder preparation, compression, and sintering. All the samples produced with this method are polycrystalline. Details of mechanical alloying will be described in the section 2.1.3.

## Chapter 2

### Literature review

#### 2.1 Cu-Al-Ni shape memory alloys

Among the various SMAs systems, (Ti-Ni-, Cu-, and Fe-based), the Cu-based system is more attractive for practical applications due to its affordable cost compared with Ti-Ni alloys and high SME compared with the Fe-based alloys [11-13]. To date, the most frequently studied Cu-based SMAs are two ternary alloys: Cu-Zn-Al and Cu-Al-Ni alloys. The Cu-Al-Ni SMAs are more resistant to degradation of shape memory properties due to undesired aging effects: it is [14] reported that the Cu-Al-Ni alloy maintains its thermal stability above 100 °C [6-9]. However several disadvantages can be found in this type of alloy. For example, such an alloy has a very high elastic anisotropy. Coarse grain size is another threat to the mechanical properties of this alloy. It is documented that the typical grain size can reach 100  $\mu\text{m}$  to 1 mm for the conventional process alloys. Both of these two defects can affect the mechanical properties of the Cu-Al-Ni system SMAs, and consequently, compromise their practical use.

In principle, the SMEs of the Cu-Al-Ni SMAs are based on the properties of high temperature binary Cu-Al  $\beta$  phase with a BCC structure [15]. During cooling, the  $\beta$  phase decomposes into  $\alpha$  and  $\gamma_2$  at 565 °C. In this situation, SME cannot be obtained. To avoid this, a high cooling rate is necessary. The Martensite Starting temperature ( $M_s$ ) and Austenite Starting temperature ( $A_s$ ) can be obtained with the following empirical equation:

$$M_s(^{\circ}\text{C}) = 2020 - 45 \times (\text{wt. \% Ni}) - 134 \times (\text{wt. \% Al}) [14, 18] \quad \text{Eq. (2)}$$

$$A_s(^{\circ}\text{C}) = 2013 - 135 \times (\text{wt. \% Al}) [17] \quad \text{Eq. (3)}$$

During the martensite transformation, as the phase diagram shows in Figure 8 to 12 [15], the BCC  $\beta$  phase regions are marked with shadows. In these regions, the phases can evolve to the required martensite and enable the alloy having SME. The phase transformation corresponds strongly to the chemical composition. With the Al content above 11 %, the parent  $\beta$  phase tends to transform to  $\beta_1$  with a  $\text{DO}_3$  superlattice prior to martensite transformation. The martensite form from  $\text{DO}_3$  also has the ordered structure. Generally, two different types of martensite can be obtained due to the different contents of the Al [15]. For the Al composition between 11 % and 13 %, a  $\beta_1'$  martensite with a structure of monoclinic 18R1 structure prevails. For the Al composition above 13 %,  $\gamma_1'$  with an orthorhombic 2H prevails. Different temperatures and tensile stresses can also lead to other martensites including  $\beta_1''$  with 18R structure and  $\alpha_1'$  with a 6R structure. Moreover, increasing Al content would lead to a reduction of the martensite transformation and help forming the intermetallic compound  $\text{Cu}_9\text{Al}_4$ . The existence of Ni slows down the diffusion of the Cu and Al. Thus, choosing the right composition of Cu-13Al-4Ni can either increase the transformation temperature or stabilize the proper phase.

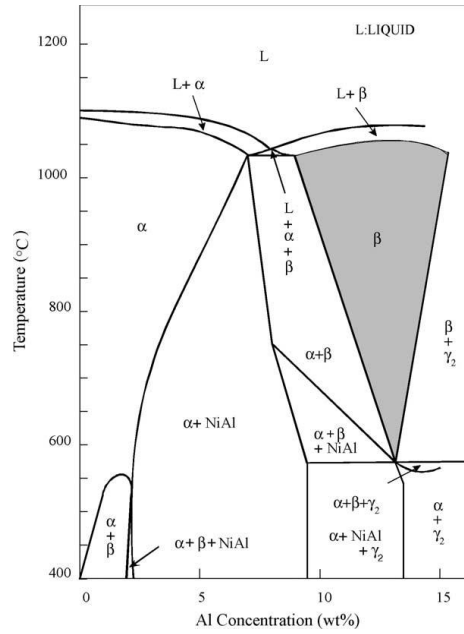


Figure 8. Binary phase diagram for the Cu-Al-Ni with the different composition of Al [15].

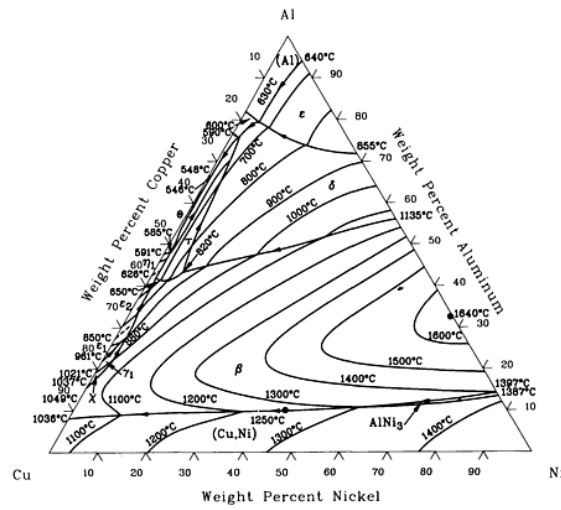


Figure 9. Ternary phase diagram of the Cu-Al-Ni at the liquid projection [16].

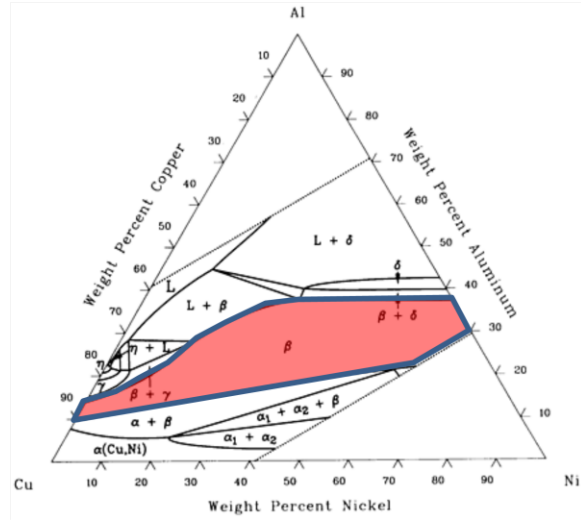


Figure 10. Ternary phase diagram of the Cu-Al-Ni at 900 °C [16].

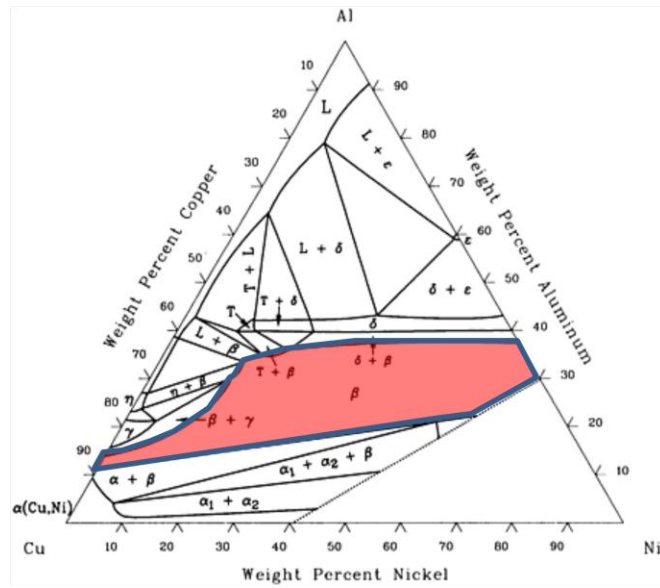


Figure 11. Ternary phase diagram of the Cu-Al-Ni at 700 °C [16].

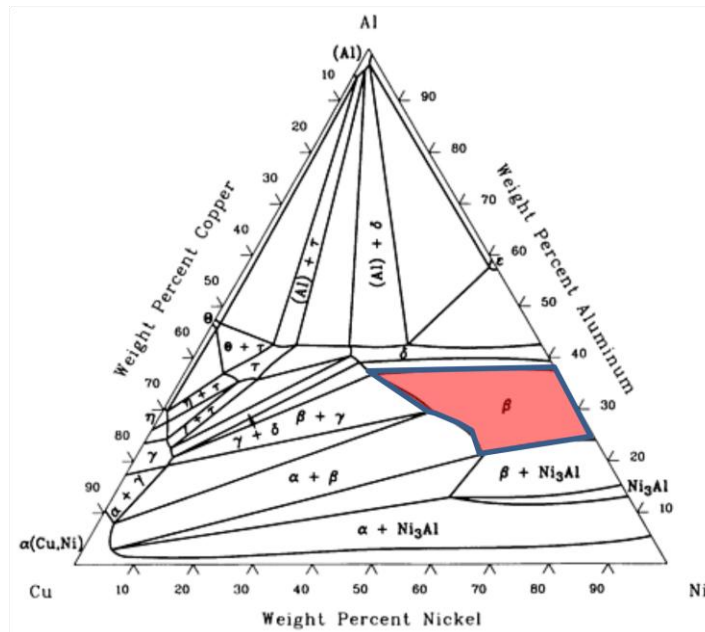


Figure 12. Ternary phase diagram of the Cu-Al-Ni at 500 °C [16].

However, the problem of the inferior mechanical properties of the polycrystalline Cu-Al-Ni alloys, which is caused by coarse grain size coupled with high elastic anisotropy, has made such alloys inferior to that of Ti-Ni-based alloys or Fe-based SMAs [2, 10-13]. The high elastic anisotropy and the large grains, which have a strong dependence of transformation strain on crystal orientation, can damage the SME by causing intergranular break-down at low average stress levels [15]. Therefore, by refining the grain size, both the mechanical properties and the SME can be enhanced. Significant effort has been carried out to improve the properties of the Cu-Al-Ni SMAs. Gastien et al. [11], Bhattacharyya et al. [15], C. Li et al. [16] reported that by fabricating the alloys into a single crystal, a significant enhancement of both mechanical properties and the SME were observed. Intensive investigation on the phase transformation within the single crystal was conducted, and different phases were fabricated for further study. Lojen et

al. [15], Itsumi et al. [17], Wu et al. [18] and Lovey et al. [3] reported that by using a rapid solidification technique, the refined grains were obtained, and thereby, the properties were improved. Zou et al. [19, 20], Fernandez et al. [21], C. Segui et al. [22] reported that introducing proper amounts of additions, the microstructure was refined, and consequently, better properties were acquired. What is more, Zengin et al. [23-25] came up with a solution and evaluation of the Cu-13Al-4Ni and Cu-13.5Al-4Ni oxidation behavior and kinetic properties by using different chemical compositions and applying different heat treatment routes.

Moreover, a series of experiments based on fabricating fine-grain sized Cu-Al-Ni SMA with mechanical alloying were conducted by Vajpai, et al. [26].

### 2.1.1 Phase and phase transformation investigation

Most of the phase investigations have been focused on the  $\beta_1$  and  $\beta_1'$ , where  $\beta_1$  is the parent phase and  $\beta_1'$  is the monoclinic 18R martensite with a parameters of  $a= 0.443$  nm,  $b= 0.533$  nm,  $c=1.297$ nm, and  $\beta=95.6$ . This phase can be stress-induced in both austenitic and martensitic SMAs [27-29].

Fernandez et al. [29] established a kinetic model of the forward and backward martensite transformations of both Cu-16.09Al-5.95Ni-0.99Ti-2.23Mn and Cu-15.6Al-5.48Ni-0.71Ti-2.12Mn SMAs for further research on the high martensite transformation temperature which could increase the potential for application.

Han et al. [30] analyzed the defects within the Cu-12Al-5Ni-1.6Mn-1Ti SMA during the reverse martensite transformation. It was observed that most defects resulted in an anomalous internal friction. It was expected that by applying stress, the negative loss of the elastic modulus could be stabilized when the orientation is unfavorable.

Gastien et al. [11] fabricated two single crystal SMAs with compositions of Cu-14.3Al-4.1Ni and Cu-14.1Al-4.2Ni. The entropy changes during  $\beta_1$  to  $\beta_1'$  transformation and  $\beta_1$  to  $\gamma'$  transformation were obtained to evaluate the changes on the relative stability of the metastable phase involved.

Cheniti et al. [32] investigated the martensite transformation within the polycrystalline SMAs for the wired Cu-13.3Al-4Ni. The result indicated a succession of two precipitates of  $\alpha_s$  and  $\gamma_2$  and the  $\alpha_s$  was inherited from nanometric globular precipitates of  $\gamma_2$  and an unsaturated  $\alpha$ .

Sari et al. [33] also investigated the microstructure of the martensite within the Cu-11.92Al-3.78Ni SMAs with SEM and TEM. Two different types of martensites (18R and 2H martensite) were identified. It was revealed that the martensites had plate group configuration. Each plate group consists of four variants. Variants A and C or B and D form spear morphology, and variants A and D or B and C form forks morphology.

Bujoreanu et al. [34] studied the  $\beta_1'$  with a decoration of  $\gamma$  phase precipitates in the Cu-13.67Al-4.28Ni-0.54Mn-0.14Fe SMA. Their work indicated that the decreased amount of  $\beta_1'$  phase usually accompanied the existence of  $\gamma$  phase. It was assumed that the strain

for the formation of  $\beta_1'$  phase acted either as a strain of the martensitic or as a strain that caused the austenitic matrix soften.

### 2.1.2 Grain refinement

As previously stated, three different solutions have been investigated to improve the mechanical properties of Cu-Al-Ni system SMAs, they are rapid cooling [35-38], precipitates introducing [40], and single crystal fabrication [41-43]. Among which, single crystal solution has been intensively studied by several research groups. Gastien et al. [11] fabricated two types of Cu-Al-Ni SMAs with single crystal, Cu-14.3Al-4.1Ni and Cu-14.1Al-4.2Ni, respectively. The as-cast single crystal SMAs were homogenized at a temperature of 1173 K, heated for 1 h, and were quenched into water at 273 K to acquire 18R and 2H martensite. A tensile test was performed to evaluate the pseudoelasticity, and the DSC was carried out. Moreover, the electrical resistance vs. temperature measurement was conducted to obtain the martensite transformation temperature. A series of tensile tests for evaluating the pseudoelastic cycles for Cu-14.3Al-4.1Ni were performed at 260, 268, and 294K, respectively. The results indicated that the ultimate tensile stress (UTS) were 70, 100, and 160 MPa, respectively. For the Cu-14.1Al-4.2Ni, the test was performed at testing temperatures of 276.5, 288, and 323.5 K, respectively, and the results illustrated the UTSs were 75, 110, and 215 MPa, respectively. Both of the 2H and 18R martensite transformation evolutions were also discussed.

Lojen et al. [15] applied rapid solidification solution to the grain refinement. In their work, Cu-Al-Ni alloy with 13 % to 15 % Al in the presence of 4 % Ni were fabricated. The melt spinning technique was performed to manufacture ultra-refined grains. After collected together from the melting spinning, the grain size was evaluated. A range of 20  $\mu\text{m}$  to 50  $\mu\text{m}$  was noted as compared to the conventional as-cast samples with grain sizes of more than 100  $\mu\text{m}$ .

Lovey et al. [27] investigated the OWSME in thin filmed Cu-26.9Al-5.5Ni SMAs. With the thin film growth technique, a nanometric mixture of  $\beta$  phase (BCC) and a consequent 2H phase were obtained irrespective of the substrate, and no SME was observed for the as-grown-film. By annealing at 1023 K for 3600 s and quenched to room temperature, an 18R martensite was acquired, and an incomplete shape recovery was observed. The SME could not reach 100 % owing to permanent plastic deformation.

Zou et al. [19] introduced traceable precipitates to enhance the mechanical property of the Cu-Al-Ni SMAs. The existence of the precipitates improved the mechanical properties with the pinning effect. The Cu-11.9Al-5Ni-1.6Mn-1Ti alloy was also investigated. Different martensites were identified by microscopic compositional analysis. The evolution of the martensite was also discussed. It was investigated in this particular material that the phase followed the M18R to N18R to N9R structure (disordered bainite precipitates) route at 300 to 350  $^{\circ}\text{C}$  for 7.2 ks.

Segui et al. [31] fabricated a polycrystalline alloy with a nominal composition of Cu-11.9Al-4.8Ni-1.0Ti, and the characterization of a hot-rolled sample with different hot

rolling temperatures and different heat treatment routes were investigated. Also, special attention was given to the change of mechanical properties and internal friction.

Sari et al. [12] studied the impact of the deformation and the mechanical properties of the conventional Cu-11.92Al-3.78Ni SMAs. In their experiment, different heat treatment routes were applied, and the influence of the heat treatment on mechanical properties was evaluated.

Zhu et al. [35] prepared a novel single crystal with a composition of Cu-13.5Al-4.5Ni-1.0Be, comparing with the conventional Cu-14Al-4Ni and Cu-12.5Al-0.5Be SMAs. With these alloys, with no cycling training, a maximum recovery strain of 10 % was obtained, implying that such SMA could be a substitution of Ti-Ni-based SMA.

Bhattacharyya et al. [36] aimed at improving the actuation for the Cu-13.3Al-4Ni single crystal SMAs by studying the effect of a temperature 100 °C higher than  $A_f$  on cyclic isothermal martensite transformation. Their research showed that at an over-heating temperature (50 °C above  $A_f$ ), the initial cyclic response is primarily shape memory whereas the subsequent cyclic response is primarily PE.

Zengin et al. [23] studied the oxidation behaviors and kinetic properties of the Cu-13Al-4Ni and Cu-13.5Al-4Ni SMAs, It was found that by increasing the content of Al, the oxidation rate was significantly reduced, which was due to a lower reaction energy is required for forming AlO than the other oxide (CuO, Cu<sub>2</sub>O). Therefore, the Al<sub>2</sub>O<sub>3</sub> were obtained and formed a condensed oxidation layer to prevent further corrosion.

### 2.1.3 Mechanical alloying

Mechanical alloying has received considerable attraction in recent decades [44-48]. Tang et al. [44] investigated the Cu-14Al-4Ni SMA with mechanical alloying, much earlier than the other researchers. Unlike the other groups, their fabrication used cold compaction, while Li's research showed that hot extrusion may lead to better results.

Li et al. [28] fabricated Cu-12Al-5Ni-2Mn with various powder metallurgy techniques, and 100 % SE was observed compared to the conventional Cu-Al-Ni SMAs with a shape recovery of 68 % after 100 cycles of deforming and recovering. In a later article, Li et al. [80] fabricated Cu-11.9Al-5Ni-2.2Mn SMA, with essentially the same powder metallurgy route, and a more intensive investigation was conducted.

Vajpai et al. [26] developed Cu-13.7Al-4.19Ni SMAs via hot densification rolling of argon atomized powder preforms. With different variants of powder metallurgy routes, a grain size less than 100  $\mu\text{m}$  was obtained. Hot rolled Cu-13.7Al-4.19Ni SMA exhibited very small grain growth during heat treatment at 950 °C up to 4h. This was explained by the pinning effect of the nano-sized alumina segregated on the grain boundaries. In their later work [68], the authors adjusted the composition to Cu-14Al-4Ni, and they used short-time ball milling, preform preparation, sintering of preforms, and hot-densification rolling of unsheathed sintered powder preforms. With this route, a more homogeneous alloy was obtained.

#### 2.1.4 Other research

Zengin et al. [49] started some innovative work by investigating the influence of neutron irradiation on the CAN SMAs. The material these authors were using was Cu-13Al-4Ni. DSC, ERC (Electrical Resistivity Changes), XRD and Visual Light Microscope (VLM) were performed on the samples. It turned out that the forward and reverse temperatures of martensite transformation and austenitic transformation were decreased after neutron irradiation.

#### 2.2 Cu-Zn-Al system

Cu-Zn-Al alloy is another commercially used SMA that is already in use practically. It has gained wide-spread interest in industry due to its particular properties, such as better TWSME compared with the other copper-based SMA (Cu-Al-Ni, Cu-Al-Be). The SME and damping properties are as good as Cu-Al-Ni system SMAs [50-55].

Ternary phase diagram are presented in Figures 13 to Figure 23 at different temperatures [56]. The marked  $\beta$  phase regions indicate the BCC austenite.



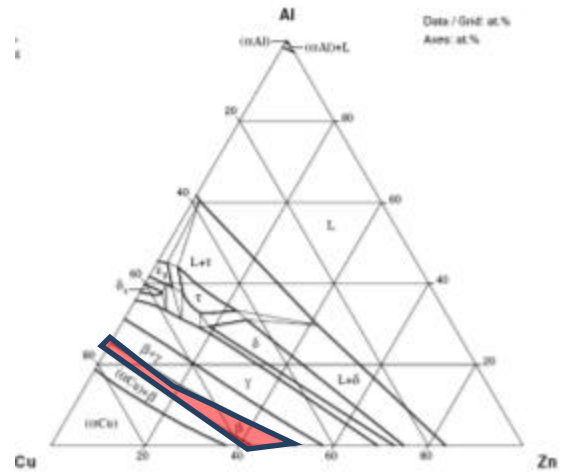


Figure 15. Ternary phase diagram of the Cu-Zn-Al at 650 °C [56].

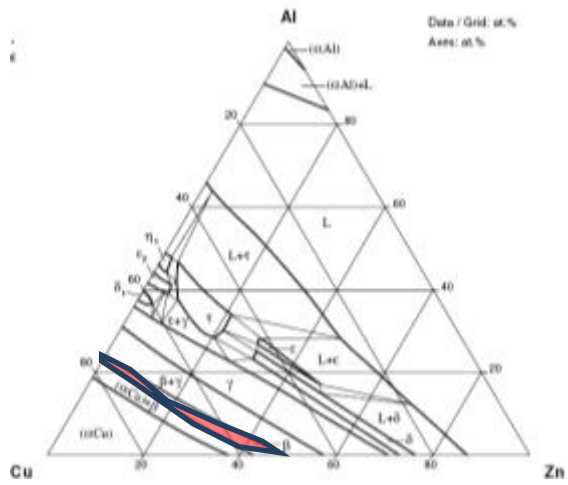


Figure 16. Ternary phase diagram of the Cu-Zn-Al at 600 °C [56].

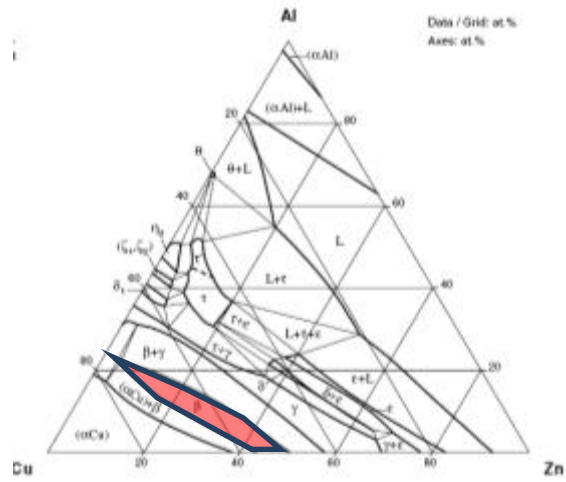


Figure 17. Ternary phase diagram of the Cu-Zn-Al at 550 °C [56].

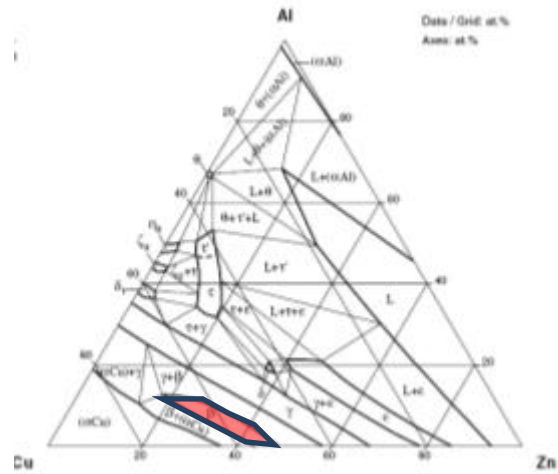


Figure 18. Ternary phase diagram of the Cu-Zn-Al at 500 °C [56].



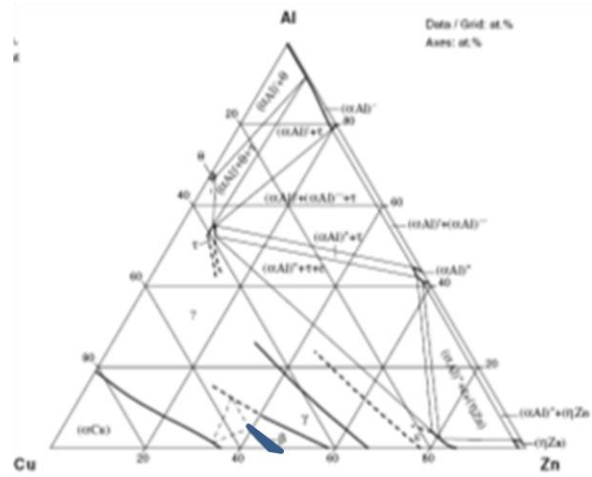


Figure 21. Ternary phase diagram of the Cu-Zn-Al at 300 °C [56].

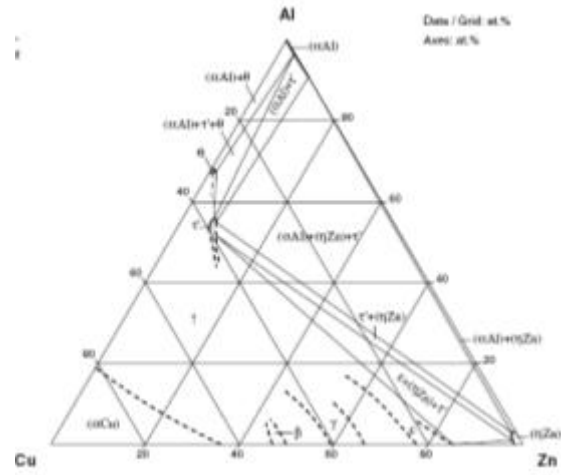


Figure 22. Ternary phase diagram of the Cu-Zn-Al at 240 °C [56].

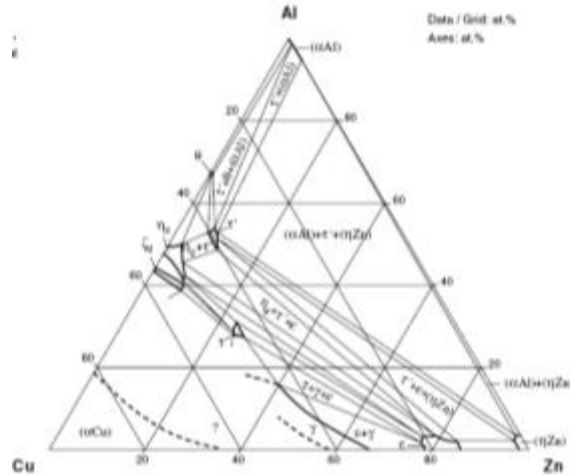


Figure 23. Ternary phase diagram of the Cu-Zn-Al at 200 °C [56].

From Figure 13 to 23, the phase diagrams show the evolution of  $\beta$  phase (shadow area) during cooling. At a relatively high temperature (around austenite temperature), the CZA with a certain composition (shadow area) can form a  $\beta$  phase, and martensite can be formed when quenched down to room temperature. Generally, there are three types of martensites inherent in the  $\beta$  phase: 6R, 18R, and 2H structures. Which phase prevails is dependent upon the electronic concentration  $e/a$ : for the  $e/a$  around 1.48, the 9R or 18R structure prevails; for the  $e/a$  below 1.48 (around 1.4), the 6R or 12R structure prevails; and for the  $e/a$  above 1.5, the 2H structure prevails [37, 57].

Longauer et al. [47] studied the Cu-Zn-Al system in the microstructural field. The samples they prepared are Cu-22Zn-4Al and Cu-22Zn-6Al. Both OWSME and TWSME were investigated.

Just as in Cu-Al-Ni system, the single crystal Cu-Zn-Al SMAs were fabricated either to enhance the material properties or to establish a more theoretical investigation in the martensite transformation.

Lexcellent et al. [43] did thorough work on the Cu-25.63Zn-4.2Al SMA in studying the thermomechanical behavior and micromechanical-based constitutive model to describe the single crystal behavior with hysteresis loops.

Sade et al. [44], a coworker of F. Lovey who studied the Cu-Al-Ni, also did considerable work on the Cu-Zn-Al. In their early work, the compositions used were from Cu-23.8Zn-12.06Al to Cu-14.55Zn-16.73Al. As soon as the alloy was fabricated, a series of heat treatments were conducted to ensure that the alloy had an 18R martensite exclusively at room temperature. Since this research focused on the microstructural evolution in the pseudoelastic cycling, the pseudoelastic cycle through the BCC to 18R martensite transformation was applied. Their work indicated that during the cycling, the defects in the bulk as well as on the surface were observed. Also, in their work a transition in the type of formed defects found in the material corresponded to an increase in the dislocation arrays parallel to the habit plane of the transformation as the test temperature increased. In their later work [45], the TWSME of the same material was also investigated with single crystal. The pseudoelastic cycling was conducted at a very low temperature to prevent defects and to disregard diffusion. By using microstructure analysis to determine phase transformation occurred within the material, the TWSME was discussed [45].

Cuniberti et al. [38, 39] investigated the different martensites with a single crystal Cu-Zn-Al SMA. The virgin materials they fabricated were Cu-12.17Zn-17.92Al and Cu-8.54Zn-21.75Al, respectively, and both 18R and 2H martensites were investigated. Their research indicated that for 18R martensite, which was a long-range ordered close-packed structure inherited from the  $\beta_1$  thermodynamically stable phase at high temperature, the antiphase boundary joining the superpartial dislocations increased its width during annealing. As for the 2H, two 2H variants were mainly investigated, which were comparable with those induced by tension from 18R single crystal.

The TWSME is one of the most important properties that has drawn considerable attentions among the material researches; much effort has been devoted to this aspect.

Pons et al. [41] investigated conventional thermomechanical cycling to establish a more intensive correlation between the procedure and the TWSME. The virgin materials they used were Cu-16.9Zn-7.7Al as single crystals, and Cu-15.8Zn-8.3Al as polycrystalline SMA. Two training protocols were investigated.

Larochette et al. [40] were seeking a solution to enhance the TWSME by refining the grain size, and in their work, they compared three different samples with different compositions and different grain sizes: Cu-13.5Zn-17.3Al and Cu-14.1Zn-16.9Al were single crystal, Cu-14.94Zn-16.53Al was coarse-grained polycrystal with a grain size of 1 to 3 mm, Cu-18.94Zn-13.95Al was fine-grained polycrystal with a grain size of 0.2 to 0.3 mm, Cu-17.99Zn-13.78Al was fine-grained polycrystal with a grain size of 0.3 to 0.8 mm representing single crystals, fine-grained polycrystals were obtained by adding grain

refiners including Co and B; and coarse-grained polycrystals were used without grain refiners. Results showed that the single crystal had the largest transformation strain.

Banerjee's et al. [42] discovery is important as well. Their investigations were carried out to understand the reasons behind the degradation of TWSME. The material used was Cu-13.39Zn-18.02Al SMA. They found that the degradation of TWSME was due mainly to aging effects envisaged in continuous transformation cycling, and the dislocations may be the main reasons for the TWSME after 200 cycles. The transformation fatigue was due to the chemical effects including the formation of precipitates of the Cu-Al.

Longauer et al. [47] investigated both the OWSME and the TWSME of Cu-22Zn-4Al and Cu-22Zn-6Al. By controlling the chemical composition and using different heat treatment routes, a dual phase with  $\alpha$  and  $\beta$  was obtained, and the SME was evaluated. From their work, two phenomena were observed: the paradoxical decrease of the OWSME and the TWSME with increasing volume fraction of martensite in the dual phase microstructure, and the TWSME degradation by thermal cycling increased with decreasing volume fraction of martensite.

Like the Cu-Al-Ni system, the mechanical properties were also investigated comprehensively. Bertolino et al. [46] fabricated a novel porous Cu-Zn-Al SMA with a composition of Cu-16.1Zn-7.9Al in the form of foams, and the mechanical properties of martensite in the pseudoelastic regime were investigated.

By introducing different precipitates, the change of the properties for the Cu-Zn-Al alloy was also investigated widely. Zhang et al. [48] studied the impact of the  $\gamma$  precipitates

on the TWSME in the Cu-23.87Zn-4.32Al. By training with the stabilization of the stress-induced martensite, the  $\gamma$  precipitates were observed to be shaped as ellipsoid within the austenite phase, and in the martensite field, the precipitates' shape changed from ellipsoid to spheroid. By doing this, the strain field was relaxed and, subsequently, benefited the TWSME.

Banerjee et al. [49] reported the effect of two different precipitates: one is produced by introducing a small amount of Ti, the SME of the Cu-12.8Zn-8.84Al-0.1Ti may be degraded although the Ti is a popular grain refiner in Cu alloy manufacture. It is reported that although the formation of the  $\text{Cu}_2\text{AlTi}$  precipitate was not detrimental to the SME. The other precipitate is  $\text{Cu}_5\text{Zn}_8$ . The formation of the  $\text{Cu}_5\text{Zn}_8$  precipitates during the aging process can impair the accommodation mechanism in the base alloy.

Also, some other properties have been investigated. Pelegrina et al. [50] studied with calorimetry the four kinds of Cu-Zn-Al samples with compositions of Cu-16.49 at. % Zn-15.75 at. % Al and Cu-8.83 at. % Zn-22.09 at. % Al, respectively. The remarkable finding was that the transformation to 2H in the polycrystalline samples would not go to completion, on the other hand, this behavior was not observed for the transition to 18R structure.

Hydrogen in the Cu-Zn-Al was investigated by Pelegrina et al. [51]. They studied the absorption of hydrogen on the martensite transformation of single-crystal wires of Cu-16.49 at. % Zn-15.75 at. % Al, Cu-6 at. % Zn-23 at. % Al, and Cu-12.62 at. % Zn-17.69 at. %

Al. But the most meaningful contribution is that they derived the stacking fault energy in the Cu-Zn-Al SMA expression as follows:

$$T = -104 + 265 \times (C_{Zn} + 1.77 \times C_{Al}) \left( \frac{mJ}{m^2} \right) \quad Eq. (4)$$

The mechanical alloying was conducted in the Cu-Al-Ni system. Zhang et al. [52] fabricated the Cu-25.5 at. % Zn-5.5 at. % Al and Cu-21.1 at. % Zn-11.2 at. % Al by powder metallurgy. In their work, microhardness was significantly increased with this technique.

### 2.3 Cu-Al-Mn system

In 1995, Kainuma et al. [58-60] have found that the Cu-Al-Mn alloy with Al content less than 18 at. % exhibited a remarkable SME property. Such a property is realized by the martensite transformation of cubic  $\beta_1$  phase ( $L_{21}$ ) to  $\beta_1'$  (6M). Moreover, the parent  $\beta_1$  phase possesses a low degree of order.

The  $M_s$  was derived by Zak et al. [61], with the following equation:

$$M_s (K) = 1192 - 225 \times Al \text{ wt. \%} - 732 \times Mn \text{ wt. \%} \quad Eq. (5)$$

The Cu-Al-Mn-based SMA with its excellent cold workability and the high fatigue strength, has drawn more and more attention in both the academic and industry fields [56].

The inventors, Kainuma and his coworkers Satou et al. [53-58] have investigated this material in different aspects. In 2003, Sutou et al. [53] studied the characterization and the application of the Cu-Al-Mn in SE, OWSME, TWSME, damping property and LTE. One

year later, they reported their work on the impact of grain size and texture on the damping properties of this alloy. In this work, four alloys were investigated, namely Cu-17Al-10Mn, 99.8 (Cu-17Al-10.2Mn) -0.2B, 98 (Cu-17.5Al-8.5Mn)-2Ni, 97.9 (Cu-17.5Al-8Mn)-2Ni-0.1Si. All the numbers indicate at. %, in the wire form, respectively. This work indicated that the damping property was dependent on the relative grain size  $d/t$  ( $d$  is the grain size,  $t$  is the wire diameter), and the development of texture that enhanced the damping capacity, moreover, high damping material with a high tensile strength over 850 MPa at room temperature were acquired. In almost the same time, the grain size and texture on the PE had also been investigated on the Cu-Al-Mn wire SMAs [55]. The materials used were Cu-17Al-10Mn, 99.8 (Cu-17Al-10.2Mn) -0.2B, 98 (Cu-17.5Al-8.5Mn)-2Ni, and 97.9 (Cu-17.5Al-8Mn)-2Ni-0.1Si. They reported several discoveries: firstly, in Cu-Al-Mn-based SMA wire with a random texture, the yield stress, the work-hardening rate, the stress hysteresis, the transformation strain, and the maximum PE recovery strain are strongly dependent upon the relative grain size ( $d/t$ ). Secondly, the  $\langle 110 \rangle$  recrystallization fiber texture was produced and enhanced by the addition of Ni. Thirdly, the orientation dependence of the “modified” Taylor factor and Schmid factor in the Cu-Al-Mn-based SMA were accompanying the  $\beta_1$  to  $\beta_1'$  transformation. Three years later, the same group reported their discovery on the effects of aging on both the thermally-induced martensite transformation [56] and the stress-induced martensite transformation [54]. In this study, they used only Cu-16.6Al-9.3Mn-2Ni-0.2B. For the thermally-induced martensite transformation, several results were presented: firstly, the hardness of the material was increased by increasing the temperature of the bainitic

transformation. Experiment showed that the hardness of the sample was increased by aging at 473, 523 and 573 K. This phenomenon was due to the formation of fine bainite plates possessing six-layered monoclinic structure in the 6M structure. Secondly, the kinetics of bainitic transformation was described by the Arrhenius equation. Thirdly, the martensite transformation temperature decreased progressively with bainitic transformation, due to composition changes within the  $\beta$  phase by atomic diffusion. Additionally, the martensite transformation intervals and hystereses increased due to the presence of the bainite plate. As for the stress-induced martensite transformation, it was reported that the Young's modulus, the critical stress of the stress-induced martensite transformation, the stress hysteresis, and the tensile strength were increased, while the tensile elongation decreased by aging, which was the consequence of the increment in the number of bainite plates. Moreover, the impact of the temperature on uniaxial stress was decreased with the progress of the bainite transformation, owing to the formation of the bainite phase.

Some other researchers also investigated these properties with different compositions. For example, Riehemann et al. [59] used Cu-11.4 to 12.3Al-5.0 to 6.9Mn; Kozlova et al. [60] used Cu-13.5Al-4.5Mn and Cu-12.4Al-5.03Mn; Wang et al. [62] used Cu-7.28Al-8.25Mn and Cu-15.41Al-8.86Mn.

It is also documented that by the year 1995, Zak et al. [61] had already developed this SMA and had investigated the SME at room temperature.

## 2.4 Cu-Al-Be system

This system of alloy was first discovered during the year 1993 by Belkhala et al. [62]. A small amount of Be was added into the Cu-Al alloy to enhance the SME. Such alloy was drawing a growing interest among the industry due to its intermediate and low temperature applications. The additive of Be could significantly decrease the transformation temperature without modifying the concentration of the eutectic point [63].

### 2.4.1 Phase and phase transformation investigation

Balandraud et al. [64] devoted considerable effort into revealing the martensite microstructure with different temperature variations. Infrared thermography was used for this purpose. It was observed that the martensite was partially transformed into stress-induced martensite because of the mechanical load. With the presence of the stress-induced martensite, a small cyclic loading was applied, and two thermomechanical couplings were observed, the thermoelastic coupling and the latent heat. This is due to the small cyclic movement of austenite-martensite interfaces. Thereafter, the martensite microstructure distribution was observed.

Kaouache et al. [65] investigated the martensite transformation intensively. Both single crystal and polycrystal samples were studied. Some PE tests were also performed. It was confirmed that the martensite transformation generated an important local stress field, and that the grain threshold stress transformation depends strongly on the orientation.

#### 2.4.2 Property improvement

Lara-Rodriguez et al. [66] applied rapid solidification to the Cu-Al-Be SMAs, and a melt spun ribbon was obtained. It was observed that the grain sizes were greatly refined. The transformation hysteresis grew as cooling rate increased.

Juan et al. [63] investigated the role of impact of the heat treatment and the related transformation behavior of this alloy. An optimized heat treatment route was derived so that the alloy could avoid both stabilization and precipitation.

Cuniberti et al. [67] investigated the relationship between grain size and PE. It was observed that the  $M_s$  stress, the PE, and the stress hysteresis decreased as the grain size increased. It was noted that the impact of the grain size on the  $M_s$  stress was much stronger than any other SMAs including Fe-based and Ni-Ti-based.

Candido et al. [68] studied the characterization of the Cu-Al-Be SMAs with an additive of Cr. A significant improvement in the mechanical properties was observed with a 0.2 % Cr composition, and the grain size was greatly refined with such composition. However, no same phenomenon was observed with other compositions of Cr.

#### 2.4.3 Other methods

To achieve a refined grain size, Ma et al. [69, 70] applied the equal channel angular pressing (ECAP) into the Cu-base SMA field. Both the mechanical property and the microstructure evolution had been studied. It was reported by their work that after 8

passes of ECAP, the  $\gamma_2$  phase was obtained and the  $\beta_1'$  with the 18R structure disappeared, however, no SME test was performed.

## 2.5 Other systems

It is also reported that some other copper base alloys could exhibit SME in some cases including Cu-Al-Be, reported by Cuniberti et al. [63], and Cu-Al-Ag, reported by Guilemany et al. [64]. Neither system was examined thoroughly, nor had these alloys been applied to industrial manufacture. Further research should be done to evaluate these SMAs.

## 2.6 Conclusions

There are four primary different systems of copper-base SMAs, including the Cu-Al-Ni system, the Cu-Zn-Al system, the Cu-Al-Mn system, and the Cu-Al-Be system. The first two systems have been applied in practical manufacture, and the others remain in the research stage. Still, much needs to be done including enhancing the mechanical properties of the copper-based SMA so that they can be more widely used as engineering material and solving the phase stability issue.

## Chapter 3

### Experimental

#### 3.1 Objectives

Since the Cu-Zn-Al is one of the most well-established Cu-based SMA systems, this alloy was selected for this research.

To reduce the cost of the alloy manufacture, conventional casting was applied in this research. With this technique, the as-cast sample is polycrystalline copper-based SMA. From the previous research, it has been noted that the mechanical properties for this alloy are relatively weak compared with other SMAs (Fe-based and Ni-Ti-based SMA). To eliminate this defect, age hardening was applied for the current study to obtain one-dimensional  $\text{Cu}_2\text{MnZn}$  precipitates. It can be expected that the existence of this precipitate will strengthen the pinning effect in the matrix, with the result that the material should exhibit better mechanical properties.

##### 3.1.1. Composition effect

To fabricate a copper-based SMA with improved mechanical properties of yield stress and ultimate tensile stress, three mechanisms, including grain refinement, lamellar structure hardening and the precipitate hardening, have been taken into consideration. The first two mechanisms will be described in the section 3.1.2. For precipitate hardening, some elements were introduced into the matrix. Extremely small uniformly-dispersed particles of second phase will form within the master alloy. The pinning effect

of the precipitates will enhance the hardness and yield strength of the material, and, consequently, the mechanical properties can be enhanced.

### 3.1.2. Structure hardening

The total hardness and strength of the material are also enhanced by the grain size. It is universally recognized that by refining the grain size, both the hardness and the yield strength can be improved. The grain size is refined by applying proper grain refiner. By introducing certain grain refiners, if the grain refiner has a similar lattice parameter and packing factor, the newly formed phase will be coherent with the matrix and assist the nucleation of the grains during solidification. Consequently, by increasing the total amount of the nuclei, the grain size can be expected to be refined significantly.

Another method for structural hardening is by applying lamellar structure. The composition of the alloy is carefully determined from the phase diagram. The eutectic point is selected to be the ideal composition, in-as-much for the eutectic structure (lamellar structure), both the  $\alpha$  phase and  $\gamma$  phase would form simultaneously during cooling. This can prevent hot tearing (hot tearing is typically caused by the residual stress resulting in different solidification rates within the material). For single crystals material, the existence of the lamellar structure can strengthen the material at the oriented directions, but for the vertical directions, there would be no such contribution for this particular structure, causing the single crystals to have different mechanical properties at different orientations. However, for the polycrystalline material, since the orientations are random, it can be expected that the mechanical properties in all the

directions would be enhanced. Since the material fabricated is polycrystalline, and the orientation lamellas in each grain are randomly aligned, it can be expected that this type of structure would enhance the whole material in all the directions.

### 3.1.3. Shape memory effect

The shape memory effect can be obtained by the electronic concentration. The electronic concentration, as it is stated, can directly influence the specific martensite that formed during the quenching process. Different electronic concentration results in different martensites including 9R Martensite, 2H Martensite. The electronic concentration relates to the outer shell electron number for different elements and compositions of the alloy. Using the concept equation, since only the electrons in the outer shell of the atoms can jump out of the shell, the electronic concentration is the total amount of free electrons divided by the total amount of atoms [4]. For the compositions in this experiment, using the following equation, the electronic concentration can be obtained from Equation 6:

$$\frac{e}{a} = \frac{(Cu \text{ at. \%} \times 1) + (Zn \text{ at. \%} \times 2) + (Al \text{ at. \%} \times 3) + (Mn \text{ at. \%} \times 2)}{Cu \text{ at. \%} + Zn \text{ at. \%} + Al \text{ at. \%} + Mn \text{ at. \%}} \quad Eq. (6)$$

Equation 6 indicates that for the Cu-Zn-Al alloy, the electronic density reaches 1.45. When Mn is added to fabricate Cu-Zn-Al-Mn alloy, the electronic density reaches 1.47. As stated previously, it can be expected that there would be more 18R martensites in the Cu-Zn-Al and more 12R martensites in the Cu-Zn-Al-Mn alloy.

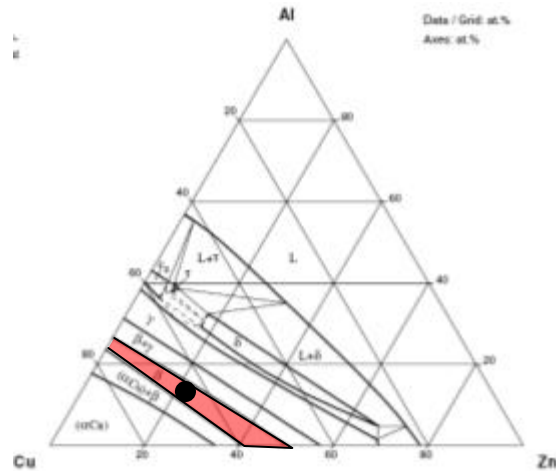


Figure 24. Phase diagram of CZA at 700 °C [56].

To sum up, a certain composition that can enable the material to have eutectic structure and to have SME should be determined. From the phase diagram (Figure 24), the shadowed region indicates  $\beta$  phase at the temperature of 700 °C, and the black dot (composition is Cu-21Zn-6Al) marked area meets the requirement.

### 3.2 Device setup

An induction furnace was used in this study. The materials were placed into a small crucible, and the crucible was placed into a ceramic vial. The whole vial was placed into a quartz glass tube, and an inert gas (Ar) was introduced into the bottom of the glass tube and exited from the other end. The glass tube and the vial were placed in the coil of the induction furnace and heated. The device is shown in Figure 25.



Figure 25. Photograph of the conventional inert gas protection setup for the induction casting.

In the experiment, to exclude the influence of impurities within the alloy, high-purity metals were used for the alloy development. The material used for casting was the 99.9 wt. % pure copper, 99.99 wt. % pure Zn, 99.99 wt. % pure Al, 99.9 wt. % pure Mn. The melting points for each pure metal are 1083 °C, 419.6 °C, 660.4 °C, 1245 °C, and 1662 °C, respectively.

### 3.3 Parameter evaluation and assessment

Solidification method:

Since  $\alpha$  copper is an FCC structure, the atomic close-packed plane should be {111}. Therefore, at this plane, there is the lowest surface energy, and during the start of the solidification process, it will be easier to form a solidified phase. During the whole solidification process, however, it is not the  $\langle 111 \rangle$  where the dendrites grow. Instead, the dendrites always grow following the  $\langle 110 \rangle$  direction [91]. This is because during the solidification, when the first interface solidifies, the sides of the formed phase (111) will

have a lower surface energy following this direction. Besides, during solidification, different interfaces with different orientations will affect each other and prevent the atoms from growing on the close-packed plane interface.

Three different solidification processes have been evaluated: water quenching, air cooling and crucible cooling. Water quenching involved pouring a very small amount of melt directly into water at room temperature. Air cooling method involves pouring a small amount of melt into a beaker at room temperature, and crucible cooling involved keeping the molten metal inside the crucible and keeping the crucible in the furnace that had been shut down.

For the water quenching, the cooling rate is relatively higher than the other two methods when the sample is in the same or similar shape and size. Because the melt is cooled down at such a high cooling rate, the grains will not have sufficient time to grow, and are trapped within a small area, which can produce a material with ultra-refined grains. The as-poured sample has an irregular shape since when the sample was poured into water, the water evaporated and when the vapor encountered the solidifying metal, it might be trapped within the metal, forming bubbles within the sample, and, subsequently, produced an irregular shape. The product of the water-quenched sample is shown in Figure 26:



Figure 26. Water-quenched Cu-Zn-Al alloy sample.

The microstructure of the sample processed with water quenching is illustrated in Figure 27.



Figure 27. Microstructure of the as-casted eutectic Cu-Zn-Al, x40.

From Figure 27, it can be seen that the grains are almost hexagonal in shape; this is due to the smaller surface energy associated with hexagonal alignment during the solidification process.

For conventional air cooling, it can be estimated that the cooling rate is higher than that for furnace cooling, but is lower than that for the water quenching. This produces more time for the grains to grow than that for the water-quenched samples, and, consequently, the grains should be much coarser. However, in this case, the sample was sprayed from the liquid phase into the air, which gave the melt an extremely high cooling rate because the amount that had been sprayed into the air was very small and cooled down fast. The as-poured samples are very small and are in pieces as it is shown in the Figure 28.

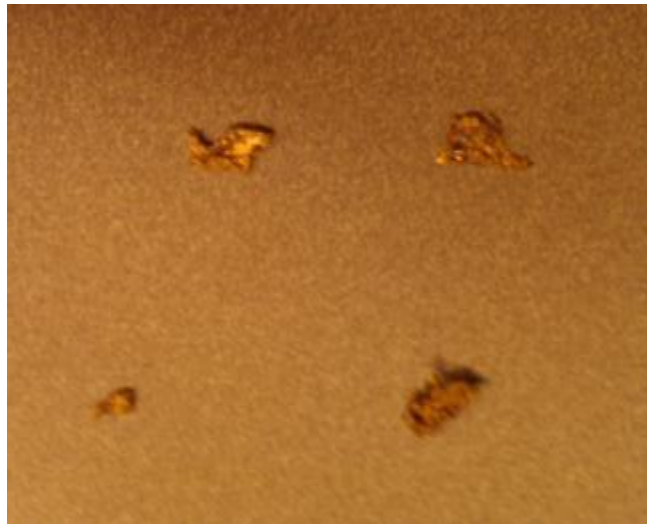
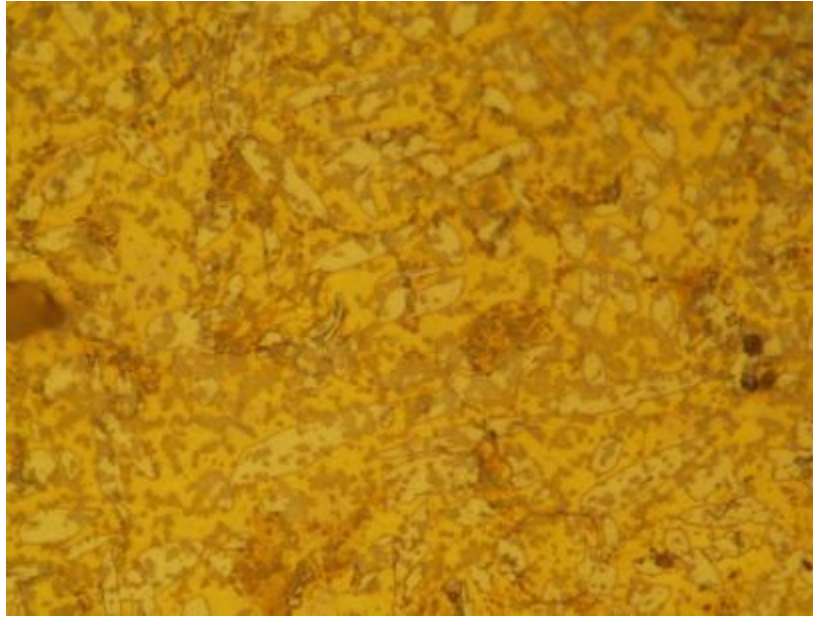


Figure 28. Air cooled as-casted Cu-Zn-Al samples.

The microstructure of the sample processed with water quenching can be seen in the following Figure 29.



**Figure 29. Microstructure of the air cooled Cu-Zn-Al alloy, x80.**

From this photograph, it can be observed that the grains are much smaller than that of the water quenching. This is because, in this particular case, the size of the sample used for the air cooling was much smaller than that of the water quenching. The samples cooled at an extremely high rate, like spray-forming for making metallic glasses. The dark spots distributed across the photograph are the micro-voids within the sample generated during the solidification process in air.

For furnace cooling, the cooling rate is the lowest among all of the three solidification methods. Therefore, it can be expected that the sample will have the coarsest grains

The microstructure of the sample processed with water quenching can be seen in Figure 30.

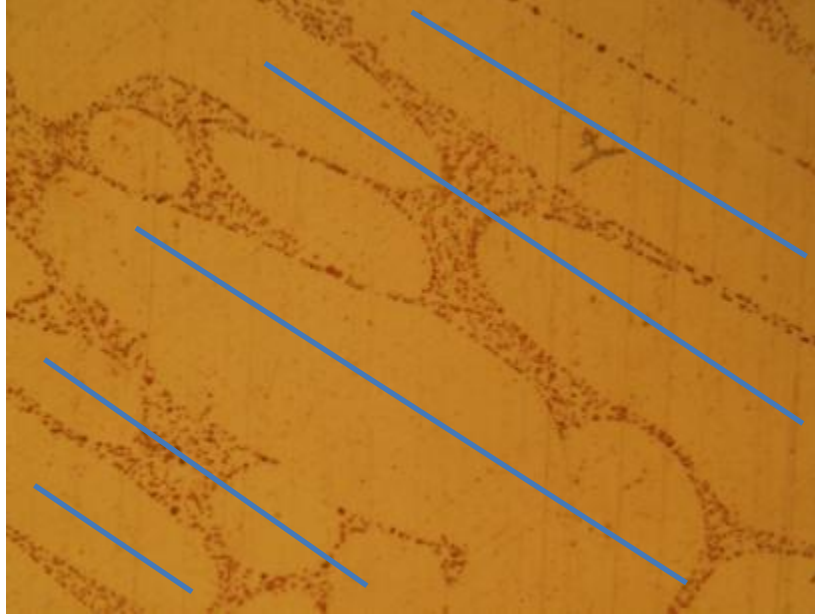


**Figure 30. Microstructure of the furnace cooling Cu-Zn-Al alloy, x40.**

From Figure 30, it can be observed that the grains have some parallel orientation. This suggests that during the solidification process, the cooling rate was relatively slow giving the grains sufficient time to grow in the direction with the lowest surface energy. The formation of such structure is due to the temperature gradient during the solidification process. During furnace cooling, the area closest to the wall of the crucible solidified first, while the inner volume of the sample was still in the liquid phase. The temperature difference between these two volumes could result a temperature gradient. The grains nucleated first and grew following the temperature gradient.

### 3.4 Rolling process evaluation

The as-cast samples were rolled to produce copper alloy strips for the shape memory effect test. Since the yield strength of the copper alloy is not as good as that of steel or aluminum alloy, the copper-based SMA before heat treatment was very easy to break down during rolling. To prevent failures, the rolling reduction percentages were manipulated under a preset level, and after each pass, the samples were annealed to remove the residual stress. The annealing temperature and time were well controlled to prevent grain growth which might be detrimental to the latter mechanical properties.

Three different rolling solutions were evaluated, with rolling reduction percentages of 8 %, 5 % and 3 %, respectively and the annealing temperature was set at 300 °C with an annealing time of 15 min.

The pre-rolled samples were cut into 6.5 mm thick cubes with the band saw, with water cooling. All the samples were rolled to 0.3 mm. The specific rolling data can be found in Table 2:

Table 2. Rolling parameters.

8 %		5 %		3 %		Continue				
Pass	Depth after Rolling(mm)	Pass	Depth after Rolling(mm)	Pass	Depth after Rolling(mm)	8 %	5 %	3 %	4 %	
1	6.5	1	6.5	1	6.5		51	0.500142	51	1.417425
2	5.98	2	6.175	2	6.305		52	0.475135	52	1.374902
3	5.5016	3	5.86625	3	6.11585		53	0.451378	53	1.333655
4	5.061472	4	5.572938	4	5.93238		54	0.42881	54	1.293645
5	4.656554	5	5.294291	5	5.7544		55	0.407369	55	1.254836
6	4.28403	6	5.029576	6	5.58177		56	0.387001	56	1.217191
7	3.941308	7	4.778097	7	5.41432		57	0.367651	57	1.180675
8	3.626003	8	4.539192	8	5.25189		58	0.349268	58	1.145255
9	3.335923	9	4.312233	9	5.09433		59	0.331805	59	1.110897
10	3.069049	10	4.096621	10	4.9415		60	0.315214	60	1.07757
11	2.823525	11	3.89179	11	4.79326		61	0.299454	61	1.045243
12	2.597643	12	3.697201	12	4.64946				62	1.013886
13	2.389832	13	3.512341	13	4.50998				63	0.983469
14	2.198645	14	3.336724	14	4.37468				64	0.953965
15	2.022753	15	3.169887	15	4.24344				65	0.925346
16	1.860933	16	3.011393	16	4.11613				66	0.897586
17	1.712058	17	2.860823	17	3.99265				67	0.870658
18	1.575094	18	2.717782	18	3.87287				68	0.844539
19	1.449086	19	2.581893	19	3.75668				69	0.819203
20	1.333159	20	2.452798	20	3.64398				70	0.794626
21	1.226507	21	2.330158	21	3.53466				71	0.770788
22	1.128386	22	2.213651	22	3.42862				72	0.747664
23	1.038115	23	2.102968	23	3.32577				73	0.725234
24	0.955066	24	1.99782	24	3.22599				74	0.703477
25	0.878661	25	1.897929	25	3.12921				75	0.682373
26	0.808368	26	1.803032	26	3.03534				76	0.661902
27	0.743698	27	1.712881	27	2.94428				77	0.642045
28	0.684203	28	1.627237	28	2.85595				78	0.622783
29	0.629466	29	1.545875	29	2.77027				79	0.6041
30	0.579109	30	1.468581	30	2.68716				80	0.585977
31	0.53278	31	1.395152	31	2.60655				81	0.568397
32	0.490158	32	1.325394	32	2.52835				82	0.551345
33	0.450945	33	1.259125	33	2.4525				83	0.534805
34	0.41487	34	1.196168	34	2.37892				84	0.518761
35	0.38168	35	1.13636	35	2.30756				85	0.503198
36	0.351146	36	1.079542	36	2.23833				86	0.488102
37	0.323054	37	1.025565	37	2.17118				87	0.473459
38	0.29721	38	0.974287	38	2.10604				88	0.459255
		39	0.925572	39	2.04286				89	0.445478
		40	0.879294	40	1.98158				90	0.432113
		41	0.835329	41	1.92213				91	0.41915
		42	0.793563	42	1.86447				92	0.406575
		43	0.753884	43	1.80853				93	0.394378
		44	0.71619	44	1.75428				94	0.382547
		45	0.680381	45	1.70165				95	0.37107
		46	0.646362	46	1.6506				96	0.359938
		47	0.614044	47	1.60108				97	0.34914
		48	0.583341	48	1.55305				98	0.338666
		49	0.554174	49	1.50646				99	0.328506
		50	0.526466	50	1.46126				100	0.318651

The samples were first heated to 300 °C and then placed into the rolls quickly. The rolling temperature was estimated to be 100 °C. After each pass, the samples were annealed at 300 °C for 15 min. Samples were examined after every 10 passes to eliminate the errors with the calibrator.

Results show that for the 8 % reduction percentage, the sample broke into pieces after 33 passes. For the 5 % sample, after 61 passes, there were a number of cracks propagated, but the sample was still in one piece. For the 3 % sample, after 102 passes, no cracks or voids were observed at the surface of the sample. The samples are illustrated in Figure 31 and 32.

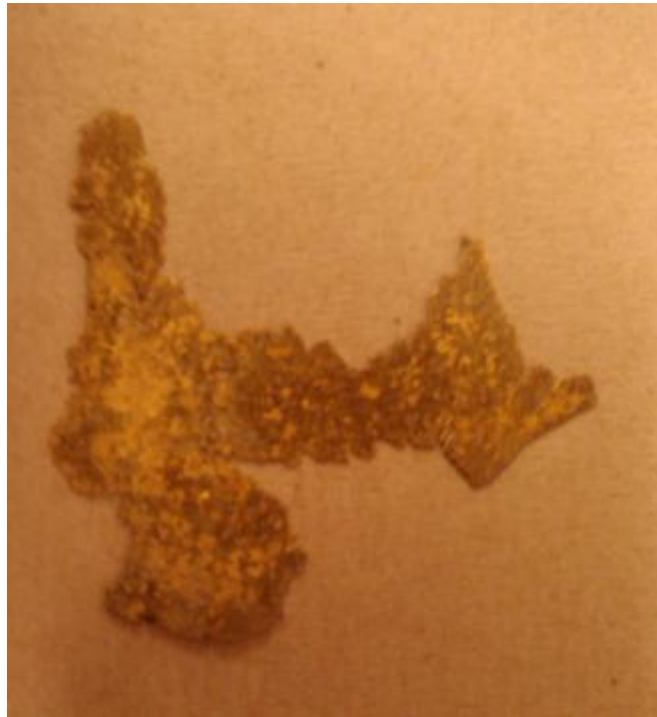


Figure 31. As-rolled Cu-Zn-Al alloy with a rolling reduction percentage of 5 %.



Figure 32. As-rolled Cu-Zn-Al-Mn alloy with a rolling reduction percentage of 3 %.

### 3.5 Heat treatment

After hot rolling, all of the samples were heat treated. The objective of the heat treatment was to solutionize the sample to obtain homogeneous compositions and to make the samples in the austenite phase for further martensite transformation. To reach the austenite phase, the samples were put into a pre-heated furnace at 650 °C. To acquire the proper solutionization time, different heat treatment times were tested and evaluated.

Since the copper-based alloy can be oxidized easily, the sample was placed in a ceramic vial. Prior to the heat treatment, some waste copper was placed into the furnace to

react with the residual oxygen inside the furnace. Since the air within the furnace had a much higher temperature than that outside, it can be assumed that the inside of the furnace was an oxygen-poor environment.

The residual oxygen may also cause oxidation on the samples. The oxidation rate can be modeled with the Matano solution [92]. The schematic diagram is shown in Figure 33.

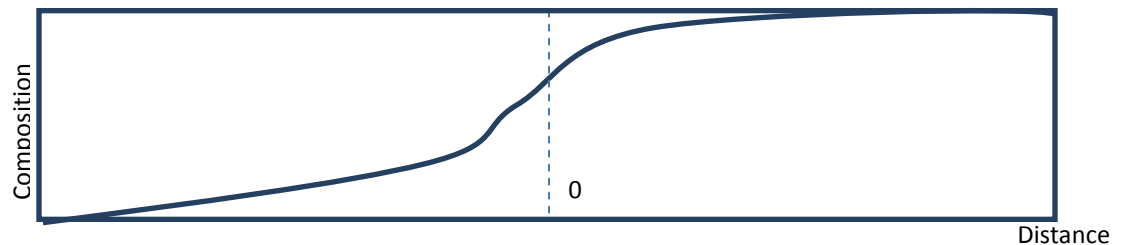


Figure 33. Schematic diagram of the Matano solution.

To model the oxidation process, a variable of the diffusion coefficient should be assumed since the oxygen compositions within the alloy would influence the diffusion coefficient. A series of assumptions were made:

No temperature changes occurred during the whole process;

In the air, the composition of the oxygen was assumed to be 21 %;

No oxygen was present within the metal;

All the metals were oxidized.

The diffusion coefficient was only a function of time and composition of oxygen.

The boundary condition and initial condition in this case is when  $t=0$ ,  $C=0$ ;  $t=\infty$ ,  $C=20.4$  %, for the alloy with a composition of Cu-21Zn-6Al, assuming all the material is

oxidized. The oxides for the materials are CuO, ZnO and Al<sub>2</sub>O<sub>3</sub>, and the composition of the oxide is 73CuO·21ZnO·3Al<sub>2</sub>O<sub>3</sub>. Therefore, the total concentration of the oxygen in these oxides is 20.1 %, with t as time, T as temperature, D as the diffusion coefficient, and C as the composition of oxygen.

Using Fick's 2<sup>nd</sup> law, we have:

$$\frac{\partial C}{\partial t} = -D \frac{\partial^2 C}{\partial x^2} \quad Eq. (9)$$

Using the Boltzman-Matano method, and defining u as the Boltzman factor, we have:

$$u = \frac{x}{\sqrt{t}} \quad Eq. (10)$$

With some mathematic transformations, we have:

$$-\frac{u}{2t} \frac{dC}{du} = \frac{\partial}{\partial x} \left( D_c \frac{1}{\sqrt{t}} \frac{dC}{du} \right) \quad Eq. (11)$$

Since the c and t are independent variables, the equation can be rewritten as:

$$-\frac{1}{2\sqrt{t}} \int_0^{20.1\%} x dC = D_c \sqrt{t} \frac{dC}{dx} \Big|_0^{20.1\%} \quad Eq. (12)$$

The curve of the diffusion can be estimated as a formula in the form of  $c = ax^2 + bx + w$ , where a, b, w are constants. With the equation above, using the Matano method and the boundary condition, the relationship of a, b and w can be estimated as:

$$2.25 \times a + 1.5 \times b = -w$$

$$w = 20.1$$

By measuring the weights of the as-heat treated sample and the same sample that had been polished to remove the oxide, the specified weight of oxide can be calculated. For the sample that was air cooled, the weight difference of two-hour heat-treated sample was 0.007 g. Therefore, it can be estimated that  $a=0.307$  and  $b= -0.41$ .

Taking a, b and c into equation 12, it can be rewritten as:

$$-\frac{1}{2}(0.153x^3 - 0.2x^2)|_0^{21.6\%} = D_c t(0.614x - 0.41)|_0^{21.6\%} \quad Eq. (13)$$

Assuming a very small value for D, in this case, D was taken as  $0.001\text{m}^2/\text{h}$ , an oxidation model was established, and the oxidation rate was evaluated.

By using this model, to obtain a 0.15 mm or less oxidation layer, the time for the heat treatment at the austenite temperature should be no longer than 4h.

The total heat treatment was evaluated with 1, 2, and 4 hrs, respectively. After that, all the samples were quenched in water at room temperature. The results are shown below:

The sample with 1h heat treatment was not oxidized completely: there were still some metallic lusters observed at the surface of the sample (Figure 34):

The sample with 2h heat treatment was covered with black oxide, and when quenched into water at room temperature, a large amount of oxide dropped-off because of the difference of the thermal expansions between the copper alloy and the oxide (Figure 35).



Figure 34. Cu-Zn-Al sample after one hour heat treatment and water quenching.



Figure 35. Cu-Zn-Al sample after 2 hour heat treatment and water quenching.

The sample with 4h heat treatment was also covered with black oxide, and when quenched into water at room temperature, the oxide was not completely removed. This is because the oxide layer was too thick on the sample to be removed through this method (Figure 36).



Figure 36. Cu-Zn-Al sample after 4 hours heat treatment and water quenching.

By comparing Figure 34 with Figure 36, the phenomenon is more clearly shown in Figure 36 (combination of the Figure 34 and 36). The second piece of sample is much darker than the first one, which means that there is more oxide on the surface of the second sample.



Figure 37. Comparison of the 1 hour heat treatment sample and 4 hour heat treatment sample.

### 3.6 Experiment details

Two materials with different compositions were developed with conventional casting. The induction furnace used in the experiment was Lepel 7-2.5-1-MC-BW induction furnace. The specific chemical composition is listed in Table 1, and the total weight for each sample developed was 20 g. Sample 1 was the Cu-21Zn-6Al, and sample 2 was Cu-21Zn-6Al-1Mn. Mn was added because it is a good grain refiner for the copper alloy, and during solidification it would benefit the pouring by increasing the castability of the sample [4]. This character is owing to the presence of a small amount of Mn during solidification, which enables the total casting product's volume to expand from the liquid phase to solid phase.

**Table 3. Composition of the samples (wt. %).**

	Cu	Zn	Al	Mn
Sample 1	Balance	21	6	-
Sample 2	Balance	21	6	1

The two as-cast samples were first heated to 300 °C for further rolling. Subsequently, the samples were hot rolled at approximately 100 °C, and a total thickness reduction of approximately 95.4 % was given to the as-cast samples. Sixty-one rolling passes with approximately 5 % thickness reduction were performed on sample 1, and 103 rolling passes with approximately 3 % thickness reduction were performed on sample 2. The samples were annealed for 15 min at 300 °C between two consecutive hot rolling passes.

The hot rolling was carried out in a two-high rolling mill. Both of the hot rolled samples were rolled into strips with thicknesses of 0.3 mm. The rolls used in the experiment was the Stanat CXBB-100 double rolls (Figure 38).



**Figure 38. Stanat double rolling mill.**

The hot-rolled strips were solutionized and homogenized at 650 °C for 2 hrs, and then water quenched.

Microstructural characterization analysis was carried out by Visual Light Microscope (VLM) and Scanning Electron Microscope (SEM). The compositions were characterized by the Energy Dispersive X-Ray spectroscopy (EDX). The samples were cold mounted with resin at room temperature to avoid grain growth caused by the temperature change. After grinding and polishing, the samples were soaked in the  $\text{NH}_4\text{OH}$  and  $\text{H}_2\text{O}_2$  solution, with a volume ratio of 1:1 for etching. The microstructures were characterized by optical microstructure.

The shape memory effect was characterized by the bend test on rod specimens with a diameter of 0.42 mm. The samples were ground to remove the residual oxide from the heat treatment process and were cut into rectangular shapes. The schematic diagram of the bending test is indicated in Figure 39.

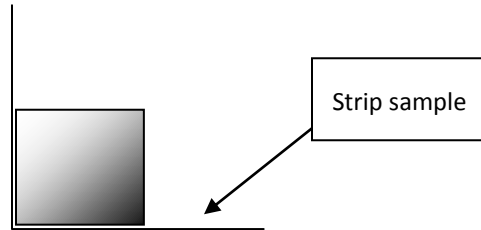


Figure 39. Schematic diagram of the shape memory effect bending test.

The shape memory effect was quantified by Shape Recovery Ratio ( $F_{SME}$ ). The  $F_{SME}$  can be expressed by the following equation:

$$F_{SME} = \frac{\vartheta_1 - \vartheta_2}{\vartheta_1} * 100\%$$

## Chapter 4

### Results

#### 4.1 Comparison of microstructures of different composition

The compositions of the two Cu-based SMAs were investigated with the EDX, respectively, as shown in Figure 40 and Figure 41:

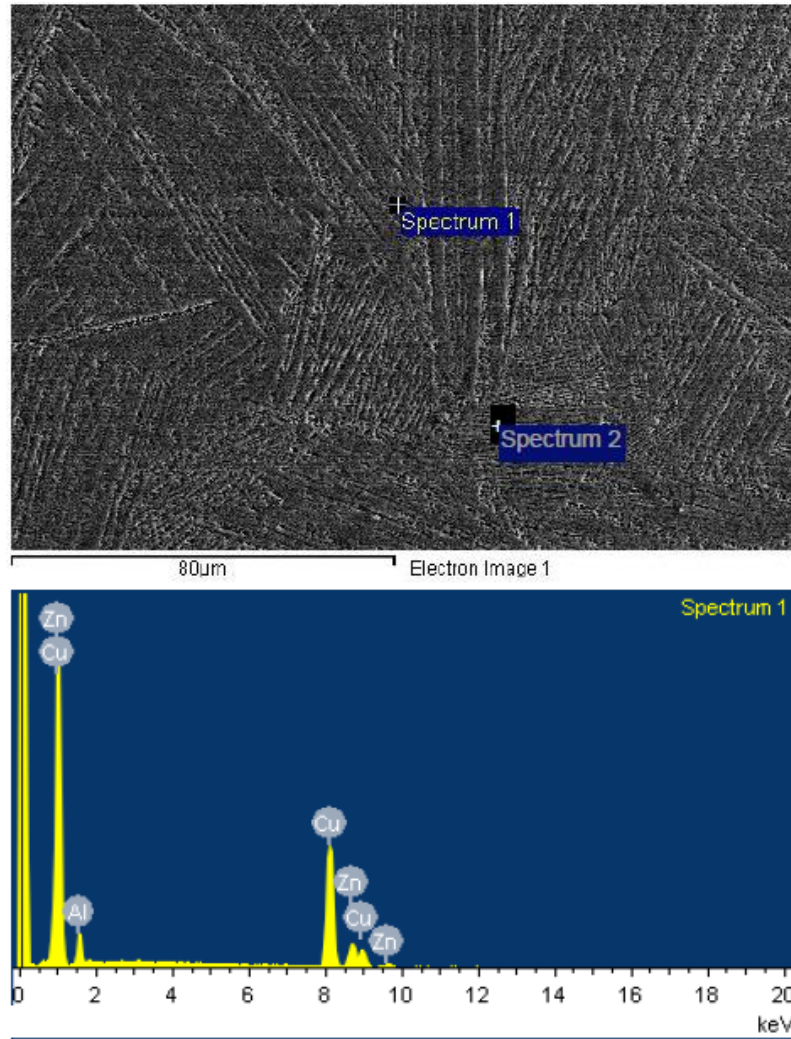


Figure 40. EDX analysis of the sample 1 (Cu-Zn-Al).

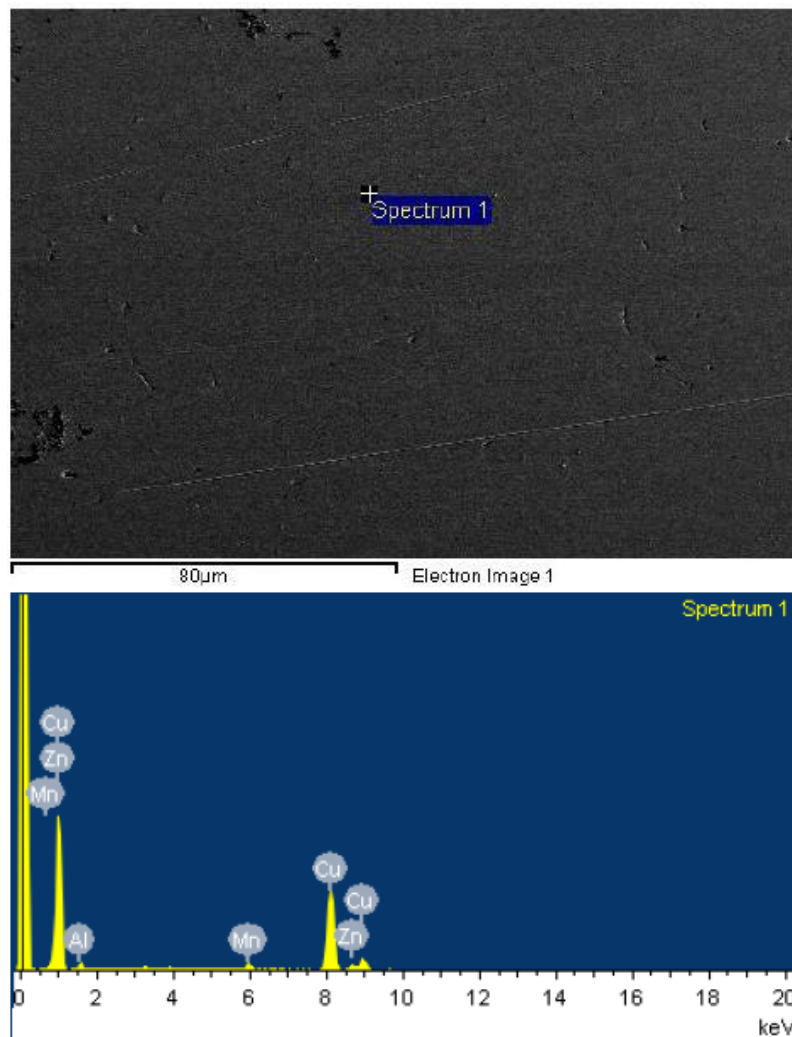


Figure 41. EDX analysis of the sample 2 (Cu-Zn-Al-Mn).

From these figures, the EDX indicates that all the chemical precursors in Cu-Zn-Al alloy and Cu-Zn-Al-Mn alloy were well diffused and homogeneously distributed in the material.

Figure 42 shows the microstructure of the as-cast sample 1. From the photograph, a clear lamellar structure is observed in the polycrystalline structure with different orientations. This is because the composition of the sample was at the eutectic point and during solidification, the two phases ( $\alpha$  phase and  $\gamma$  phase) grew cooperatively

behind an essentially planar solidification front. As the  $\alpha$  phase (Cu-rich phase) solidified, the Zn atoms were in excess and diffused laterally for a short distance. This enables the  $\gamma$  phase (Zn-rich phase) to be formed during solidification. Similarly, the Cu atoms, rejected ahead of the  $\gamma$  phase, diffuse to the tip of adjacent  $\alpha$  lamellae [88].

With this structure, the material can be reinforced along the lamellar structure. However, the lamellar structure in the vertical direction would weaken the mechanical properties. Since the material is polycrystalline, and the orientation of the lamellae varies, it can be suggested that the different lamellae will strengthen mechanical properties in all the directions, and consequently, improve the overall mechanical properties of the material.

Figure 43 shows the microstructure of the as-cast sample 2. From this photograph, very few lamellar structures can be observed, owing to the small amount of additive Mn, which caused the eutectic point to shift. The  $\alpha$  phase and  $\gamma$  phase could not be formed simultaneously then. It can be clearly seen that the grain size of sample 2 is greatly refined with the addition of Mn.



Figure 42. Microstructure of the CZA sample 1 with Cu-Zn-Al, x80.

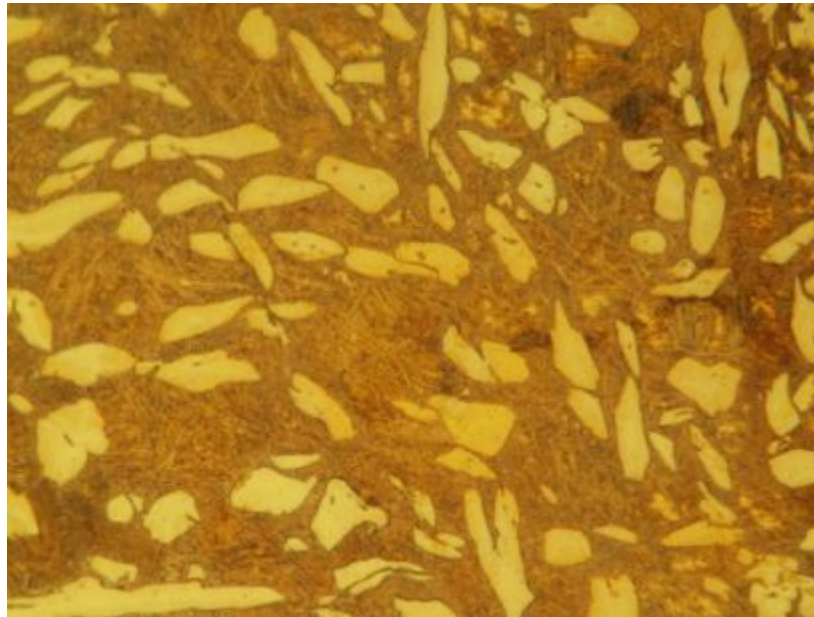


Figure 43. Microstructure of the sample 2 with Cu-Zn-Al-Mn, x80.

#### 4.2 Shape memory effect

Two bending tests were carried out on both of the samples. The results are illustrated in Figures 44, 45, 46, and 47.



Figure 44. Shape memory effect test of the sample 1 (deforming stage).



Figure 45. Shape memory effect test of the sample 1 Cu-Zn-Al (Recovering stage).



Figure 46. Shape memory effect test of the sample 2 Cu-Zn-Al-Mn (deforming stage).

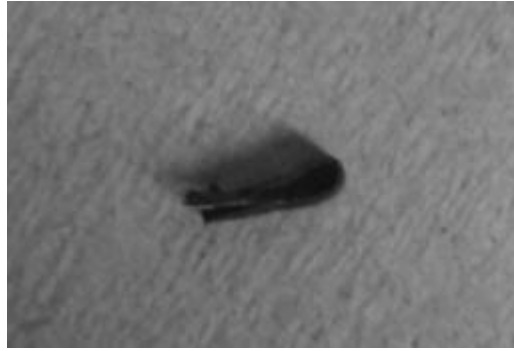


Figure 47. Shape memory effect test of the sample 2 Cu-Zn-Al-Mn (recovery stage).

For sample 1, the total bending angle was  $90^\circ$ , and after heating, the strip recovered approximately  $7^\circ$ . Therefore, the total recovery is 4%. For sample 2, the total bending angle was  $180^\circ$  and the shape recovery was 3% with an angle recovery of approximately  $5^\circ$ .

The detrimental effect of Mn on the shape memory effect is not only due to the pinning effect of the precipitates of  $\text{Cu}_2\text{AlMn}$ , but also due to lowering of the transformation and recovery temperature according to Bhuniya et al. [87].

## Chapter 5

### Conclusions

The following conclusions can be drawn from these results:

- i. A polycrystalline copper-based SMA, with a Mn additive which is different to the previous researchers, was developed, and the microstructure, as well as the shape memory effect, were investigated;
- ii. The eutectic lamellar structure in this type of alloy was fabricated. The different orientation of the lamellae in the polycrystalline material could enhance the material's mechanical properties;
- iii. The solidification process was analyzed and discussed. The reason for the Cu alloy growth in the  $\langle 110 \rangle$  direction is because that at nucleation, compared with the close-packing direction, the sides of the unit nuclei have larger surface energy. Taken these conditions, the sides of nuclei enable the atoms to attach to the nuclei prior to the other sites such as facets of the unit nuclei. Therefore, the preferred growth direction is  $\langle 110 \rangle$  [90];
- iv. An analytic method was used for determining the optimized heat treatment. It was calculated and tested that for 4 hours heat treatment, the sample was still in good condition that and could be used for the subsequent bending test;
- v. By adding 1 wt % Mn, the SME was reduced, but the mechanical properties were improved with precipitation hardening. The degradation effect is due to

the pinning effect caused by the additives. However, the shape memory effect still existed, due to the low content of the additive;

- vi. Mechanical properties, such as yield stress and hardness, are enhanced through a combination of precipitation hardening, lamellar structure, and grain refinement.

#### Future work

Reviewing previous research, it is suggested that following work should be done in the future:

- i. The specified lamellar strengthening improvement in mechanical properties need to be evaluated;
- ii. A precipitate with a better coherency needs to be introduced so that the SME can be enhanced;
- iii. The precipitates should be characterized by TEM;
- iv. Relative papers should be published.

## Reference:

- [1] D. C. Lagoudas, Shape memory alloys, ISBN 978-0-387-47684-8, 2008, pp. 4 (Book)
- [2] S. K. Vajpai, R. K. Dube, S. Sangal, Microstructure and properties of Cu–Al–Ni shape memory alloy strips prepared via hot densification rolling of argon atomized powder preforms ,*Mat. Sci. Eng. A*, 2011, pp. 378-387
- [3] F. C. Lovey, A. M. Condo, J. Guimpel, M. J. Yucaman, Shape memory effect in thin films of a Cu–Al–Ni alloy, *Mat. Sci. Eng. A*, 2008, pp. 426-430
- [4] F. C. Lovey, V. Torra, Shape memory in Cu-based alloys: phenomenological behavior at the mesoscale level and interaction of martensite transformation with structural defects in Cu-Zn-Al, *Progress in Material Science*, 1999, pp. 189-289
- [5] K. Sugimoto, *Bulletin of Japan Institute of Metals* 24 (1985) pp. 45
- [6] J. R. Davis, ASM International Handbook committee, *Copper and copper alloys*, 2001, pp. 121-126
- [7] M. Ahler, Phase Stability of Martensitic Structures, *Jour. De Physique IV*, 1995, ppC8-71-C8-08
- [8] OHBA Laboratory website  
([http://www.geocities.jp/ohba\\_lab\\_ob\\_page/structure2.html](http://www.geocities.jp/ohba_lab_ob_page/structure2.html))
- [9] C. Satto, J. Jansen, C. Lexcellent, D. Schryvers, Structure refinement of  $L_{21}$  Cu–Zn–Al austenite, using dynamical electron diffraction data, *Solid State Communications*, 2000, pp. 273-277

- [10] S. Akmak, E. Artun, Theoretical analysis of the Crystallography for  $DO_3 \rightarrow M18R$  Martensitic Transformation, Turkish Journal of Physics, 1998, pp. 139-149
- [11] R. Gastien, C. E. Corbellani, M. Sade, F. C. Lovey, Thermodynamical aspects of martensitic transformations in CuAlNi single crystals, Scripta Mat. 2004, pp. 1103-1107
- [12] U. Sari, T. Kirindi, Effects of deformation on microstructure and mechanical properties of a Cu–Al–Ni shape memory alloy, Mat. Char., 2008, pp. 920-929
- [13] Y. Sutou, N. Koeda, T. Omori, R. Kainuma, K. Ishida, Effects of ageing on bainitic and thermally induced martensitic transformations in ductile Cu–Al–Mn-based shape memory alloys, Acta Mat., 2009, pp. 5748-5758
- [14] Z. C. Lin, W. Yu, R. H. Zee, B. A. Chin, CuAlPd alloys for sensor and actuator applications, Intermetallics 8, 2000, pp. 605-611
- [15] G. Lojen, I. Anzel, A. Kneissl, A. Krizman, E. Unterweger, B. Kosec, M. Bizjak, Microstructure of rapidly solidified Cu–Al–Ni shape memory alloy ribbons, Mat. Proc. Tech., 2005, pp. 220-229
- [16] M. Zhu, X. Ye, C. Li, G. Song, Q. Zhai, J. Alloys & Compounds, 2009, pp. 404-410
- [17] Y. Itsumi, Y. Takashima, K. Kamei, K. Sugimoto, Mater. Sci. Forum 56-58, 1990, pp. 469
- [18] M. H. Wu, Bulletin of Japan Institute of Metals 24 (1985), pp. 69
- [19] W. H. Zou, H. Y. Peng, R. Wang, J. Gui, D. Z. Yang, Heating effects on fine structure of a Cu-Al-Ni-Mn-Ti shape memory alloy, Acta Mater., 1995, pp. 3009-3016

- [20] J. Gui, W. H. Zou, R. Wang, D. Zhang, C. H. Tang, M. Z. Xiang, D. Z. Yang, X-ray diffraction study of the reverse martensitic transformation in Cu-Al-Ni-Mn-Ti shape memory alloy, *Scripta Mater.*, 1996, pp. 435-440
- [21] J. Fernandez, A. V. Benedetti, J. M. Guilemany, X. M. Zhang, Thermal stability of the martensitic transformation of Cu–Al–Ni–Mn–Ti, *Mater. Sci. Eng. A*, 2006, pp. 723-725
- [22] C. Segui, J. Pons, E. Cesari, J. Muntasell, J. Font, Characterization of a hot-rolled Cu-Al-Ni-Ti shape memory alloy, *Mater. Sci. Eng. A*, 1999, pp. 625-629
- [23] R. Zengin, S. Ozgen, M. Ceylan, Oxidation behaviour and kinetic properties of shape memory  $\text{CuAl}_x\text{Ni}_4$  ( $x=13.0$  and  $13.5$ ) alloys, *Thermochimica Acta*, 2004, pp. 79-84
- [24] F. Auricchio, V. Massarotti, One-way and Two way shape memory effect, thermo-mechanical characterization of Ni-Ti wires, *Anno Accademico*, 2007/2008, pp. 6
- [25] G. Ghosh, J. V. Humbeeck, Al-Cu-Zn, *Landolt-Bornstein*, MSIT, pp. 182-204
- [26] S. K. Vajpai, R. K. Dube, S. Sangal, Microstructure and properties of Cu–Al–Ni shape memory alloy strips prepared via hot densification rolling of argon atomized powder preforms, *Mat. Sci. Eng. A*, 2011, pp. 378-387
- [27] F. C. Lovey, A. M. Condo, J. Guimpel, M. J. Yacaman, Shape memory effect in thin films of a Cu–Al–Ni alloy, *Mat. Sci. Eng. A*, 2008, pp. 426-430
- [28] Z. Li, Z. Y. Pan, N. Tang, Y. B. Jiang, N. Liu, M. Fang, F. Zheng, Cu–Al–Ni–Mn shape memory alloy processed by mechanical alloying and powder metallurgy, *Mat. Sci. Eng. A*, 2006, pp. 225-229

- [29] J. Fernandez, A. V. Benedetti, J. M. Guilemany, X. M. Zhang, Thermal stability of the martensitic transformation of Cu–Al–Ni–Mn–Ti, *Mat. Sci. Eng. A*, 2006, pp. 723-725
- [30] C. L. Gong, F. S. Han, Anomalous internal friction associated with the thermoelastic martensitic transformation in a Cu–Al–Ni–Mn–Ti alloy, *Scripta Mat.*, 2007, pp. 181-184
- [31] C. Segui, J. Pons, E. Cesari, J. Muntasell, J. Font, Characterization of a hot-rolled Cu–Al–Ni–Ti shape memory alloy, *Mat. Sci. Eng. A*, 1999, pp.625-629
- [32] M. Zhu, X. Ye, C. Li, G. Song, Q. Zhai, *Jour. Alloy & Comp.*, 2009, pp. 404-410
- [33] U. Sari, I. Aksoy, *Jour. Mat. Proc. Tech.*, 2008, pp. 72-76
- [34] S. M. Tang, C. Y. Chung, W. G. Liu, *Mat. Proc. Tech.*, 1997, pp. 307-312
- [35] H. Cheniti, M. Bouabdallah, E. Patoor, High temperature decomposition of the  $\beta_1$  phase in a Cu–Al–Ni shape memory alloy, *Jour. Alloy and Com.*, 2009, pp. 420-424
- [36] G. K. Kannarpady, S. Trigwell, A. Bhattacharyya, S. Pulnev, I. Viahi, *Mech. Mat.*, 2006, pp. 493-509
- [37] M. Ahlers, Martensite and equilibrium phases in Cu-Zn and Cu-Zn-Al alloys, *Prog. Mater. Sci.*, 1986, pp.135
- [38] A. Cuniberti, R. Romerero, A. Condo, Compression-induced hexagonal martensite in Cu–Zn–Al, *Mat. Sci. Eng. A*, 2002, pp. 177-181
- [39] A. Cuniberti, M. Niewczas, Effect of temperature on superdislocation dissociation in Cu–Zn–Al 18R single crystals, *Scripta Mat.*, 2001, pp. 853-858

- [40] P. A. Larochette, M. Ahlers, *Mat. Sci. Eng. A*, 2003, pp. 249-257
- [41] J. Pons, M. Masse, R. Portier, Thermomechanical cycling and two-way memory effect induced in Cu–Zn–Al, *Mat. Sci. Eng. A*, 1999, pp. 610-615
- [42] S. Datta, A. Bhunya, M. K. Banerjee, Two way shape memory loss in Cu-Zn-Al alloy, *Mat. Sci. Eng. A*, 2001, pp. 291-298
- [43] C. LExcellent, B. C. Goo, Q. P. Sun, J. Bernardini, Characterization, thermomechanical behaviour and micromechanical based constitutive model of shape-memory Cu-Zn-Al single crystals, *Acta Mater.*, 1996, pp. 3773-3780
- [44] J. Malarria, M. Sade, F. Lovey, Microstructural evolution in the pseudoelastic cycling of Cu–Zn–Al single crystals: behavior at a transition stage, *Mater. Sci. Eng. A*, 2001, pp. 88-100
- [45] J. Malarria, F. Lovey, M. Sade, Two way shape memory effect in Cu-Zn-Al single crystals after pseudoelastic cycling at low temperatures, *Mater. Sci. Eng. A*, 2009, pp. 118-124
- [46] G. Bertolino, P. Arneodo Larochette, E. M. Castrodeza, C. Mapelli, A. Baruj, H. E. Troiani, Mechanical properties of martensitic Cu-Zn-Al foams in the pseudoelastic regime, *Mater. Letters*, 2010, pp. 1448-1450
- [47] S. Longauer, P. Makroczy, G. Janak, M. Longauerova, Shape memory effect in a Cu–Zn–Al alloy with dual phase  $\alpha/\beta$  microstructure, *Mater. Sci. Eng. A*, 1999, pp. 415-419

- [48] X. M. Zhang, M. Liu, J. Fernandez, J. M. Guilemany, Effect of small  $\gamma$ -precipitates on the two-way shape memory effect in Cu–Zn–Al alloys, *Mater. & Design*, 2000, pp. 557-559
- [49] A. K. Bhuniya, P. P. Chattopadhyay, S. Datta, M. K. Banerjee, On the degradation of shape memory effect in trace Ti-added Cu–Zn–Al alloy, *Mater. Sci. Eng. A*, 2005, pp. 125-132
- [50] J. L. Pelegrina, R. Romero, Calorimetry in Cu–Zn–Al alloys under different structural and microstructural conditions, *Mater. Sci. Eng. A*, 2000, pp. 16-22
- [51] C. Damiani, J. L. Pelegrina, M. Ahlers, Hydrogen in Ti–Ni–Cu and Cu–Zn–Al shape memory alloys, *Jour. Alloy and Comp.*, 1999, pp. 243-250
- [52] S. Zhang, L. Lu, M. O. Lai, Cu-based shape memory powder preparation using the mechanical alloying technique, *Mater. Sci. Eng. A*, 1993, pp. 257-262
- [53] Y. Sutou, T. Omori, J. J. Wang, R. Kainuma, K. Ishida, Characteristics of Cu–Al–Mn-based shape memory alloys and their applications, *Mater. Sci. Eng. A*, 2004, pp. 278-282
- [54] Y. Sutou, N. Koeda, T. Omori, R. Kainuma, K. Ishida, Effects of ageing on bainitic and thermally induced martensite transformations in ductile Cu–Al–Mn-based shape memory alloys, *Acta Mater.*, 2009, pp. 5748-5758
- [55] Y. Sutou, T. Omori, N. Koeda, R. Kainuma, K. Ishida, Effects of grain size and texture on damping properties of Cu–Al–Mn-based shape memory alloys, *Mater. Sci. Eng. A*, 2006, pp. 743-746

- [56] ASM Handbook, 2001 vol. 3, pp. 1521-1523 (Book)
- [57] Y. Sutou, T. Omori, K. Yamauchi, N. Ono, R. Kainuma, K. Ishida, Effect of grain size and texture on pseudoelasticity in Cu–Al–Mn-based shape memory wire, *Acta Mater.*, 2005, pp. 4121-4133
- [58] R. Kainuma, S. Takahashi, K. Ishida, *Metall. Mater. Trans.*, 1996, pp.2187-2192
- [59] A. Mielczarek, N. Kopp, W. Riehemann, *Mater. Sci. Eng. A*, 2009, pp. 182-185
- [60] L. E. Kozlova, A. N. Titenko, Stress-induced martensitic transformation in polycrystalline aged Cu–Al–Mn alloys, *Mater. Sci. Eng. A*, 2006, pp. 738-742
- [61] G. Zak, A. C. Kneissl, G. Zatulskij, Shape memory effect in cryogenic Cu-Al-Mn alloys, *Scripta Mater.*, 1996, pp. 363-367
- [62] R. Wang, J. Gui, X. Chen, S. Tan, *Acta Mater.*, 2002, pp. 1835-1847
- [63] S. Montecinos, A. Cunibeti, A. Sepulveda, Grain size and pseudoelastic behavior of a Cu–Al–Be alloy, *Mater. Char.*, 2008, pp. 117-123
- [64] J.M. Guilemany, J. Fernandez, X.M. Zhang, TEM study on the microstructure of Cu–Al–Ag shape memory alloys, *Mater. Sci. Eng. A*, 2006, pp. 726-729
- [65] J. Font, E. Cesari, J. Muntasell, Thermomechanical cycling in Cu–Al–Ni-based melt-spun shape-memory ribbons, *J. Pons. Mater. Sci. Eng. A*, 2003, pp. 207-211
- [66] L. Dalaey, P. Hassen (Ed.), *Phase transformation in Materials*, VCH, Weinheim, 1991

- [67] G. K. Kannarpady, S. Trigwell, A. Bhattacharyya, S. Pulnev, I. Viahhi, *Mech. Mater.*, 2006, pp. 493-509
- [68] S. K. Vajpai, R. K. Dube, P. Chatterjee, S. Sangal, *Minerals, Metals & Materials society and ASM International 2012 (Book)*
- [69] K. Otsuka, T. Ohba, M. Tokonami, C. M. Wayman, New description of long period stacking order structures of martensites in  $\beta$ -phase alloys, *Scripta Mat.*, 1993, 1359-1364
- [70] K. Otsuka, C. M. Wayman, K. Nakai, H. Sakamoto, K. Shimizu, Superelasticity effects and stress-induced martensite transformations in Cu-Al-Ni alloys, *Acta Mat.*, 1976, 207-226
- [71] K. Otsuka, H. Sakamoto, K. Shimizu, Successive stress-induced martensitic transformations and associated transformation pseudoelasticity in Cu-Al-Ni alloys, *Acta Mat.*, 1979, 585-601
- [72] S. Stanciu, L. G. Bujoreanu, Formation of  $\beta'_1$  stress-induced martensite in the presence of  $\gamma$ -phase, in a Cu-Al-Ni-Mn-Fe shape memory alloy, *Mat. Sci. Eng. A*, 2008, pp. 494-499
- [73] S. Belkhala, F. Zuniga, H. Guenin G., *Mat. Sci. Eng. A*, 1993, pp. 169-174
- [74] P. Zhang, A. Ma, S. Lu, P. Lin, J. Jiang, H. Ma, C. Chu, *Mat. Letters*, 2009, pp. 2676-2679

[75] P. Zhang, A. Ma, J. Jiang, S. Lu, P. Lin, D. Yang, G. Liu, *Jour. Alloys & Compounds*, 2010, pp. 210-214

[76] B. Kaouache, S. Berveiller, K. Inal, A. Eberhardt, E. Patoor, Stress analysis of martensitic transformation in Cu–Al–Be polycrystalline and single-crystalline shape memory alloy, *Mat. Sci. Eng. A*, 2004, pp. 232-237

[77] C. H. Gonzalez, C. J. De Araujo, N. F. Quadros, G. Guenin, M. Morin, Study of martensitic stabilisation under stress in Cu–Al–Be shape memory alloy single crystal, *Mat. Sci. Eng. A*, 2004, pp. 253-256

[78] C. M. Wayman, *J. Met*, Fabrication of the D022-type intermetallic compound Al<sub>3</sub>Ta via powder metallurgy processes and its characterization, 1990, pp. 129-139

[79] T. Tadaki, K. Otsuka, C. M. Wauman (Ed), *Shape memory materials*, Cambridge University Press, Cambridge, 1998

[80] Z. Xiao, Z. Li, M. Fang, S. Xlong, X. Sheng, M. Zhou, *Mat. Sci. Eng. A*, 2008, pp. 266-272

[81] R. Zengin, M. Ceylan, *Mat. Letters*, 2003, pp. 55-59

[82] J. Rodriguez-Aseguinolaza, I. Ruiz-Larrea, M. L. No, A. Lopez-Echarri, E. H. Bocanegra, J. San Juan, Thermal history effects of Cu–Al–Ni shape memory alloys powder particles compared with single crystals behaviour, *Intermetallics*, 2010, pp. 2183-2190

- [83] G. A. Lara-Rodriguez, G. Gonzalez, H. Flores-Zuniga, J. Cortes-Perez, The effect of rapid solidification and grain size on the transformation temperatures of Cu–Al–Be melt spun alloys, *Mat. Char.*, 2006, pp. 154-159
- [84] I. Lopez-Ferreno, T. Breczewski, I. Ruiz Larrea, A. Lopez-Echarri, M. I. No, J. San Juan, Thermal treatments and transformation behavior of Cu–Al–Be shape memory alloys, *Alloy and Comp.*, 2012, Accepted Manuscript
- [85] G. V. M. Candido, T. A. de A. Melo, V. H. C. de Albuquerque, R. M. Gomes, S. J. G. de Lima, J. M. R. S. Tavares, *ASM international*, 2012, Accept Manuscript
- [86] S. Montecinos, A. Cuniberti, A. Sepulveda, Grain size and pseudoelastic behaviour of a Cu–Al–Be alloy, *Mat. Char.*, 2008, pp. 117-123
- [87] A. K. Bhuniya, On the degradation of shape memory effect in trace Ti-added Cu–Zn–Al alloy, *Mat. Sci. Eng. A*, 2005, pp. 125-132
- [88] D. A. Potter, K. E. Easterling, *Phase transformation in metals and alloys*, 2nd Ed., 1981, pp. 222 (Book)
- [89] Y. Sutou, N. Koeda, T. Omori, R. Kainuma, K. Ishida, Effects of aging on stress-induced martensitic transformation in ductile Cu–Al–Mn-based shape memory alloys, *Acta Mater.*, 2009, pp. 5759-5770
- [90] D. A. Porter, K. E. Easterling, *Phase Transformations in Metals and Alloys*, 2<sup>nd</sup> ed., 1992 pp. 164 (Book)

[91] C. Matano, On the Relation between the diffusion-coefficients and concentrations of solid metals. Japanese Journal of Physics, 1933

## Appendix

### Curriculum vitae:

- Born in P. R. China, Jan 5<sup>th</sup>, 1983
- Studied Material Science and Engineering, Central South University, Changsha, P. R. China, 2001-2005
- Internship in Anshan Steel Inc., 2006
- Worked in Beijing Adfaith Consulting Inc., 2007-2008
- Master of Science studied in Material Science and Engineering, Worcester Polytechnic Institute, Worcester, M. A. 2009-2011
- Ph. D studies in Material Science and Engineering, University of Nevada, Reno, Reno, N. V., 2011-now
- Vice President of Student Advantage in the ASM (America Society of Material), Worcester chapter, 2010-2011

### Academic Projects:

- **“Effect of the Mn additive on the Cu-Zn-Al Shape Memory Alloy”, Reno, N. V., 2011-2012, advisor: Qizhen Li**  
  
Improved the Cu-Zn-Al shape memory alloy with the additive of Mn, the shape memory effect was characterized and the microstructures were investigated.
- **“Characterization of Al-6Ni-xCu Alloy”, Worcester, M. A., 2010-2011, advisor: Makhoulf M. Makhoulf**

Analyzed the mechanical property on Al-Ni-Cu alloy, compared the samples that had undergone different heat treatments, determined the roles of the copper that acted in strengthening the alloy as precipitates and studied the feasibility of strengthening the Al-Ni-based alloy by precipitate hardening.

- **“Defect Analysis of Explosion Welding on TA2 Alloy”, Hunan, China, 2005, advisor: Yang Yang**

Investigated the defect morphology on the TA2 tube after the explosion welding. Stimulated the formation of the defects and explored the mechanism of all kinds of cracks and other defects in the case.

- **“Application of Dendrites Structure in Continuous Casting of Steel”, Liaoning, China, 2005-2006, advisor: Xiaohong Sui**

Studied the dendrite structure morphology under 2-dimensional scale in continuous casting condition quantitatively, compared the nucleation rate under different stirring methods; established an empirical correlation between the cooling rate and the dendrite arm space. Studied the relationship between the silicon content and the defects.

- **“Analysis on Oxidation Resistance of Cr-Zr-Cu Alloy for Continuous Crystallizer”, Liaoning, China, 2004-2005, advisor: Xiaohong Sui**

Mainly worked on data integration.

#### **Presentations:**

- X. Sui, G. Xie, B. Zhao, H. Li, "Application of Dendrites Structure in Continuous Casting of Steel", ICASI'2008 and CCATM'2008 (International Conference and Exhibition on ANALYSIS & TESTING OF MATERIALS), Beijing, P. R. China, Nov. 8<sup>th</sup>, 2008
- Haohan Li, "Characterization of the Al-6Ni-xCu alloy", Grad 2011 Graduate Students Achievement Day, MA, Apr. 15<sup>th</sup>, 2010

**Publications:**

- H. Li, Q. Li, Effect of the Mn additive on the Cu-Zn-Al Shape Memory Alloy, MS thesis, May, 2012
- X. Sui, H. Li, Analysis on Property of Oxidation Resistance of Cr-Zr-Cu Alloy for Continuous Crystallizer , Physical Test, 2007, vol 5., pp. 117-120
- X. Sui, G. Xie, B. Zhao, H. Li, Effect of Continuous Casting Process Parameters on Solidifying Structure of Low Carbon Steel Billets, Physical and Chemical Test, 2008, vol 6
- X. Sui, P. Li, G. Xie, H. Li, Macroscopically Measurement and its Application for Solidified Dendrite Structure in Continuous Cast Billet, Steel, 2009, vol 8